

1 Regulation of excitatory presynaptic activity by Ambra1 protein 2 determines neuronal networks in sex-dimorphic manner

3
4 Anes Ju^{1,2#}, Bekir Altas¹, Hong Jun Rhee¹, Manuela Schwark¹, Imam Hassouna², Albrecht
5 Sigler¹, Hiroshi Kawabe¹, Kamal Chowdhury³, Hannelore Ehrenreich², Nils Brose¹ and
6 JeongSeop Rhee^{1*}

7 ¹Department of Molecular Neurobiology, Max Planck Institute for Multidisciplinary Sciences
8 (City Campus), Göttingen, Germany

9 ²Clinical Neuroscience, Max Planck Institute for Multidisciplinary Sciences (City Campus),
10 Göttingen, Germany

11 ³Department of Molecular Cell Biology, Max Planck Institute for Multidisciplinary Sciences
12 (Faßberg Campus), Göttingen, Germany

13 [#]Current address: Samsung Advanced Institute of Technology, Samsung Electronics, Suwon-
14 si, South Korea

15
16 *Correspondence: rhee@mpinat.mpg.de

17 18 **Abstract**

19 Heterozygous mutation of *Ambra1*, known as a positive autophagy regulator, produces autism-
20 like behavior in mice and autistic phenotypes in humans in a female-specific manner. However,
21 the substantial roles of the *Ambra1* mutation in neurons are still unknown. We find that *Ambra1*
22 heterozygotes display a moderate decrease in excitatory synaptic release *in-vitro* and *ex-vivo*
23 exclusively in females without autophagy activity, resulting in significant alterations in γ -
24 oscillation power and seizure susceptibility by excitatory/inhibitory (E/I) imbalance. Specifically,
25 *Ambra1* deficiency has no effect on neurogenesis and morphogenesis, but selectively
26 decreases excitatory synaptic activity without changes in synapse number, quantal size,
27 synaptic release probability, and synaptic plasticity. Therefore, the limited excitatory
28 synaptopathy by *Ambra1* expression levels ultimately determines E/I imbalance in global
29 neural networks leading to the female-specific ASD.

30 31 **Keywords**

32 *Ambra1*, E/I imbalance, Autism, Synaptic transmission, Seizure, Oscillations, Sex-dimorphism
33

34 **Introduction**

35 Autism-spectrum disorder (ASD) is a neurodevelopmental disorder mainly characterized by
36 deficits in social interaction/communication and restricted/repetitive patterns of behavior
37 (Association, 2013). Epidemiological studies estimated that ASD has been diagnosed in more
38 than 1% of the world's population (Elsabbagh et al., 2012; Vos et al., 2016) and described as
39 a sexually-dimorphic disease, with four times more males than females being diagnosed
40 (Baron-Cohen et al., 2011; Chakrabarti and Fombonne, 2001). Genetic etiology of ASD is
41 highly heterogenous, with greater than 100 identified risk genes involved in diverse functions,
42 such as transcriptional regulation, protein synthesis and degradation, synapse function and
43 synaptic plasticity (Bourgeron, 2015; Delorme et al., 2013; Ebert and Greenberg, 2013).
44 Whether genetically distinct forms of ASD share common pathophysiology at the neural
45 network level still remains to be elucidated.

46 Emerging evidence has suggested a disturbed homeostasis of excitatory/inhibitory (E/I)
47 balance as an etiology of ASD (Nelson and Valakh, 2015; Zikopoulos and Barbas, 2013).
48 Epilepsy, relatively high comorbidity in ASD, occurring in 5-38% of autistic individuals,
49 highlights the possibility of shared neurophysiological mechanisms involved with changed
50 neural network activities ("Epilepsy and autism spectrum disorders may have a shared
51 aetiology," 2016; Lee et al., 2015). This hypothesis is corroborated by electroencephalogram
52 (EEG) abnormalities often observed in patients with ASD or epilepsy (Martinerie et al., 1998;
53 Mathalon et al., 2015; Rossi et al., 1995; Spence and Schneider, 2009), addressing that altered
54 neuronal network and synchronicity are related with those two diseases. Based on several
55 mouse studies proposing sexually dimorphic mechanisms regulating neural circuits (Li et al.,
56 2016; Malishkevich et al., 2015), E/I balance is a critical factor of ASD in a sexually-dimorphic
57 manner. However, the neurophysiological substrates of E/I imbalance in ASD still stimulates
58 our curiosity.

59 Ambra1 (activating molecule in Beclin1-regulated autophagy) is a crucial regulator in
60 autophagy, proliferation and apoptosis in eukaryotic cells (Maria Fimia et al., 2007).
61 Homozygous mutation of *Ambra1* gene in mice (*Ambra1*^{gt/gt}) resulted in embryonic lethality
62 showing neural tube defects (Maria Fimia et al., 2007). Interestingly, *Ambra1* heterozygous
63 mice (*Ambra1*^{+/gt}), that are viable, produced clear autism-like behaviors only in females, which
64 might be linked to sexually-dimorphic expression of Ambra1 protein in brain tissue (Dere et al.,
65 2014). Additionally, our previous study showed early brain enlargement and different seizure
66 propensity depending on developmental stages in this mouse line in a female-specific manner
67 supporting *Ambra1*^{+/gt} mice as a model of female-specific ASD (Mitjans et al., 2017). Especially,
68 this study includes human genetic research reporting a significant association between autistic

69 features and intronic single nucleotide polymorphisms of the *AMBRA1* gene in females but not
70 in males. Therefore, *Ambra1* heterozygous mice is proved as a construct-valid genetic mouse
71 model of female ASD (Mitjans et al., 2017).

72 The present study has been designed to explore the neural substrate underlying this E/I
73 balance observed in the brains of *Ambra1*^{1+gt} females by screening functional and
74 morphological aspects of neural network in brain slice. In addition, in order to define the precise
75 role of the *Ambra1* protein, we studied the functional consequences by the absence of *Ambra1*
76 gene in autaptic neuronal culture of *Ambra1* homozygous mutation. Our study revealed that
77 *Ambra1* present in the brain was limitedly located in neuronal cells, and was particularly
78 accumulated in the synapses. We found that, regardless of sex, *Ambra1* was directly involved
79 in excitatory synaptic activity, while showing no effect on neuronal development and synapse
80 formation. More importantly, it was noticed that the reduction of excitatory synaptic activity by
81 *Ambra1* heterozygosity only in females, although not significant, is a decisive cause of synaptic
82 E/I input imbalance, contributing to ASD.

83

84 **Results**

85 Region-, cell type- and subcellular-specific expression of *Ambra1* protein

86 We first analyzed the expression pattern of *Ambra1* protein in region, different cell types and
87 subcellular location of mouse brain. mRNA expression data from Allen brain atlas revealed
88 that *Ambra1* is widely present (Figure 1A). Histochemical or immunofluorescent staining of β-
89 galactosidase (β-gal) in mouse brains showed that *Ambra1* is abundantly expressed in cortex,
90 striatum and hippocampus and in neurons, but not in glial cells (Figure 1B-E). Subcellular
91 fractionation of *Ambra1*^{1+/-} cortex (Figure 1F) (Bermejo et al., 2014), where the purification of
92 synaptic membrane was validated (Figure 1G), was used for Western Blot of *Ambra1* protein.
93 Surprisingly, *Ambra1* protein was identified not only in ER-Golgi enriched fractions (P2B) but
94 also in crude synaptic membrane (CSM) and pure synaptic membrane fractions (SM, Figure
95 1G). These data illustrate that *Ambra1* protein is located only in neurons and is particularly
96 distributed in synapses, suggesting a possibility of its role in neuronal communication.

97

98 No change in activity-dependent synaptic plasticity upon *Ambra1* heterozygous mutation

99 Due to neuronal expression and synaptic location of *Ambra1* protein, we sought to determine
100 the consequences of *Ambra1* heterozygous mutation in neural networks for learning and
101 memory. Based on previous studies showing the modification of synaptic plasticity and
102 oscillatory activity in several ASD mouse models (Hammer et al., 2015; Mathalon et al., 2015),
103 we recorded them in acute hippocampal slices from 4 week-old mice before sexual maturation

104 (Heiniger H. J. and Dorey, 1989), using extracellular recording. Overall, we found the input-
105 output curve, paired-pulse ratio, and early-phase long-term potentiation (Figure 2) were
106 comparable between two genotypes in male and female mice, pointing out that, upon *Ambra1*
107 heterozygous mutation, activity-dependent synaptic activities and plasticity are unaltered.
108

109 *Perturbed γ-power and seizure propensity by Ambra1 heterozygous mutation only in females*
110 *but not in males*

111 To specifically and concretely measure the local activity of neural network, we assessed the
112 oscillatory activity in hippocampal CA3 pyramidal layer induced by Kainate. The peak
113 frequencies were detected within γ-range (25-45 Hz) and comparable between two genotypes.
114 Intriguingly, the average power of γ-oscillation was significantly lower in *Ambra1^{+/gt}* females
115 compared to control littermates, while male mice exhibited similar levels between two
116 genotypes (Figure 3D-E), indicating female-specific alteration of synchrony of neural network
117 activities in *Ambra1^{+/gt}* brains.

118 Epilepsy, one of the comorbid conditions of ASD (Bolton et al., 2011), is a behavioral feature
119 manifested by abnormal synchrony of neural network activities (Sun et al., 2021). The seizure
120 threshold was markedly higher in *Ambra1^{+/gt}* females compared to control, which is shown by
121 earlier latency of whole-body seizure episodes and higher seizure score, whereas those
122 parameters were similar between two genotypes in males (Figure 3F-G). Taken together,
123 higher seizure propensity and lower power of gamma oscillations in heterozygous females
124 demonstrate that female mice are more sensitive to disturbed synchronous network activity
125 upon *Ambra1* heterozygous mutation.

126

127 *E/I imbalance by change in functional excitatory synapses, regardless of autophagy activity*

128 To investigate the cellular substrates underlying the E/I imbalance which is the significant
129 mechanism causing the abnormal synchronization in a neuronal network, we first compared
130 the population of excitatory and inhibitory neurons between two genotypes. The densities, sum
131 and ratio of the mature glutamatergic (CTIP2+) and GABAergic (GAD67+) neurons as well as
132 the density of parvalbumin-expressing (PV+) interneurons were similar in pyramidal layer of
133 hippocampus between *Ambra1^{+/+}* and *Ambra1^{+/gt}* female mice (Figure 4A-G). This data
134 suggests that the *Ambra1* heterozygous mutation is not crucial for neuronal proliferation and
135 apoptosis, which are not a main factor for the alteration in γ-oscillation power in this mouse
136 line.

137 By Western blotting with the anti-LC3 antibody, LC3-II/LC3-I ratio, an indicative of autophagic
138 activity, was similar between *Ambra1^{+/+}* and *Ambra1^{+/gt}* in female cortical homogenates (Figure
139 4H-I). This is corroborated by unaltered expression levels of different synaptic proteins in

140 hippocampal homogenates or cortical synaptosomal fractions between two genotypes (Figure
141 S1). Therefore, our data imply that the autophagic activity of *Ambra1* unaccompanied by
142 neuron is not a critical factor in the E/I imbalance.

143 We measure miniature excitatory and inhibitory postsynaptic currents (mEPSC and mIPSC) at
144 the same neuron in acute brain slice and morphological features by simultaneously filling the
145 recorded neurons with biocytin, as a minimal functional model system (Figure 3A).

146 The morphological properties of hippocampal pyramidal neurons, including dendritic
147 arborization and number of mushroom spines (Figure 5A-C), were unaltered by *Ambra1*
148 heterozygous mutation, which is additionally supported by independent experiments using *in*
149 *utero* electroporated samples (Figure S2). Moreover, PSD95 and Gephyrin as well as
150 PSD95/Gephyrin expression, implying the number of excitatory and inhibitory post-synapses
151 and their ratio, were not altered in *Ambra1^{+/gt}* brains (Figure S1C-D). Similar neuronal
152 morphology and expression levels of postsynaptic proteins can infer that the number of
153 excitatory and inhibitory postsynapses were unchanged by *Ambra1* heterozygous mutation.

154 Without changes in mEPSC and mIPSC amplitudes, only mEPSC frequencies of female
155 *Ambra1^{+/gt}* neurons showed a strong tendency for reduction (Figure 5D-F), suggesting that the
156 possibility due to a decrease in the number of functional glutamatergic synapses cannot be
157 excluded. Surprisingly, the ratio of frequencies of mIPSC and mEPSC, which indirectly
158 described the cellular E/I balance, was significantly increased in *Ambra1^{+/gt}* females compared
159 to control littermates, while male mice showed a similar trend without significance (Figure 5E).

160 These data indicate that the ratio of excitatory and inhibitory inputs into single cells can be a
161 critical factor in network homeostasis (Huang et al., 2021; Xue et al., 2014) rather than the
162 change in the number of overall inputs themselves.

163 Subtle phenotypes of synaptic function by *Ambra1* heterozygous mutation lead to further
164 analysis of synaptic release by the absence of *Ambra1* gene. We accessed the synaptic
165 release property of glutamatergic autaptic neurons cultured from cortex of *Ambra1⁺⁺*,
166 *Ambra1^{+/gt}* and *Ambra1^{gt/gt}* embryonic littermate in both sexes, at embryonic day 14.5 just
167 before embryonic lethality (Figure 6). Since it was unlikely to obtain three genotypes of both
168 sexes from the same littermates, the data from mutant neurons were normalized by the ones
169 of *Ambra1⁺⁺* neurons from their littermates.

170 Evoked EPSC (eEPSC) amplitude and total number of synaptic vesicles ready to release,
171 called readily releasable pool (RRP), in *Ambra1^{gt/gt}* neurons were reduced to ~67% in male
172 and ~51% in female, respectively, of control values without change in mEPSC amplitudes and
173 vesicular release probability (P_{vr}) (Figure 6A-D), suggesting that *Ambra1* is essential for the
174 activity of excitatory synapse. Interestingly, even in these cultured neurons grown
175 independently and separately, the most prominent alteration depending on sex is that the

176 eEPSC and RRP sizes in female heterozygous neurons, exhibited a decreasing trend, but not
177 in males (Figure 6A-D). Synaptic plasticity upon 10 Hz stimuli was similar between three
178 genotypes (Figure 6E-F). Interestingly, both sexes exhibited approximately 30% of reduction
179 in response to exogenous application of glutamate in *Ambra1^{gt/gt}*, which is different from the
180 change in synaptic responses (Figure 6C-D).

181 We tested whether the reduction of eEPSC amplitude is due to defects in synaptogenesis by
182 the absence of Ambra1. Using immunofluorescent staining of vGluT1 and PSD95 to label
183 glutamatergic pre- and postsynapses in each autaptic neuron, the number of presynaptic and
184 postsynaptic puncta were similar between genotypes, and Mander's overlapping coefficient
185 between vGluT1 and PSD95 signals were comparable between genotypes, indicating that the
186 spatial integrity of pre- and postsynapses were unaffected by Ambra1 (Figure S3). This
187 indicates, even in cultured single neurons, sex-dimorphic changes in synaptic release were
188 detected without alteration in synaptic number, as data in acute brain slices. In order to find
189 out whether the phenotype also occurs in inhibitory input, the similar analysis was performed
190 in autaptic GABAergic neurons cultured from the striatum of female mice at postnatal day 0
191 (Nair et al., 2013). Interestingly, the release machinery and synaptic GABA receptor cluster
192 was not changed in *Ambra1^{+/gt}* neurons (Figure 6G). Our data addressed that *Ambra1*
193 heterozygous mutation produces a pronounced effect restricted to glutamatergic release in
194 females without any environmental factors.

195

196 **Discussion**

197 We characterized the consequence of *Ambra1* heterozygous mutation, known to induce
198 female-specific ASD, by multiple level of analysis including behavioral, biochemical,
199 morphological, and electrophysiological approaches. The remarkable and distinct finding in
200 our study is that the reduced power of γ -oscillations and increased susceptibility to seizure in
201 *Ambra1* heterozygous mice, two proxies of E/I imbalance, occurs exclusively in females
202 (Figure 3). To understand the mechanism underlying this imbalance, we considered the
203 possible contribution of autophagy that may serve as a bridge linking Ambra1 and ASD. This
204 is because autophagy has been known to have a profound relationship with neurodegenerative
205 diseases caused by the accumulation of harmful proteins and damaged organelles and
206 neuronal development diseases such as ASD caused by impairment of neurodevelopmental
207 processes including neurogenesis, neuronal differentiation and synaptic remodeling/function
208 (Gkogkas et al., 2012; Kuijpers et al., 2021; Tang et al., 2014).

209 Our previous study demonstrated a marked brain enlargement in female *Ambra1^{+/gt}* mutant
210 (Mitjans et al., 2017), which is a common feature in human ASD (Courchesne et al., 2011).

211 And Ambra1 protein is also known to be involved in proliferation/apoptosis and its absence
212 induced brain overgrowth in mouse embryos (Maria Fimia et al., 2007). It further strengthened
213 the autophagy hypothesis to support the ASD seen in the *Ambra1^{+/gt}* and led us to speculate
214 that altered populations of different cell types or overgrowth of neuronal morphology, such as
215 dendritic arborization or spine density, may disturb E/I balance and contribute to brain
216 overgrowth.

217 First of all, the current study displays a novel fact that Ambra1 in the brain is only present in
218 neurons, including synapses and it limited the target of Ambra1 function (Figure 1). Moreover,
219 the number of glutamatergic, GABAergic and PV-expressing neurons, dendrite complexity,
220 and spine density is unaltered in *Ambra1^{+/gt}* hippocampal region, indicating no critical effect on
221 the neurogenesis by *Ambra1* heterozygous mutation (Figure 4A-G, Figure 5A-C and Figure
222 S1-2). Crucially, no significant difference is found in autophagic activity between *Ambra1^{+/gt}*
223 and *Ambra1^{+/+}* brains (Figure 4H-I), which could be supported by previous data that ~50% of
224 autophagic activity was still observed in *Ambra1^{gt/gt}* embryonic brains (Maria Fimia et al., 2007).
225 Therefore, it can be inferred that the cause of ASD, probably E/I imbalance in *Ambra1^{+/gt}*, is far
226 from autophagy activity, which has been known to directly affects axon and synapses (Cheng
227 et al., 2015; Soukup et al., 2016; Soykan et al., 2021; Wang et al., 2015).

228 The oscillatory activity in the neural network is a comprehensive signal of global E/I. To further
229 dissect the cellular substrates underlying the alteration of this E/I signal, we focused on
230 functional synapses rather than morphological ones. The possible cause of E/I imbalance,
231 occurring only in female *Ambra1^{+/gt}* brain slices, is a slight decrease in mEPSC frequency
232 (Figure 5E). This moderate reduction at single cell level, through altering ratio with mIPSC
233 frequency, can be accumulated at the neuronal network level, which contributes as the basis
234 for inducing ASD. That is, even small changes in the number of functional synapses or synaptic
235 activity can cause the E/I imbalance. The finding is highly reminiscent of previous study for
236 *Nlgn4* knockout mice, as a construct-valid and face-valid mouse model of ASD, proposing that
237 the accumulation of subtle local changes in synaptic function yields pronounced perturbation
238 in global network activity (Hammer et al., 2015). We projected the "little things make great
239 things" into our data. However, it was still not sufficient to explain the mechanism by which
240 ASD occurring in *Ambra1* heterozygous mutation appear only in female.

241 The female-specific behavioral phenotypes had to consider the influence of specific
242 environments *in vivo*, such as unique hormones. To study the neuronal intrinsic change by
243 genetic factors limited to females, eliminate the external effects coming from *in vivo* conditions,
244 and deconvolute the diluted results from E/I input measurement, we specifically analyzed the
245 cultured neurons from very early embryonic day 14.5 just before *Ambra1^{gt/gt}* embryos death
(Maria Fimia et al., 2007). As the intrinsic activities of cultured *Ambra1^{+/+}*, *Ambra1^{+/gt}*, and

247 *Ambra1* ^{gt/gt} neurons could be compared simultaneously, it enables us to understand the
248 substantial role of Ambra1 in neurons. As a result, regardless of sex, Ambra1 deficiency had
249 no effect on neuronal development and synapse formation, and decrease selectively the
250 number of functional glutamatergic synapses. Moreover, surprisingly, the cultured *Ambra1* ^{1+gt}
251 neurons also showed a female-specific decrease in eEPSC size, as the change in mEPSC
252 frequency in *Ambra1* ^{1+gt} female brain acute slice (Figure 6A-D). Thus, ASD caused by E/I
253 imbalance in *Ambra1* heterozygous mutation is a neuron-intrinsic property of Ambra1 by sex
254 difference without any environmental factors. And our previous study, the decrease in relative
255 Ambra1 expression level in female *Ambra1* ^{1+gt} brain, compared to one in male (Dere et al.,
256 2014), may help to understand the female-specific synaptic phenotype. Thus, we can suggest
257 that the size of EPSCs would be determined according to the expression level of Ambra1
258 protein.

259 In *Ambra1* ^{gt/gt} neurons, the comparable mEPSC amplitudes and the eEPSC or mEPSC
260 frequencies reduced in half lead to the novel fact that there are Ambra1-dependent and -
261 independent synapses. In particular, it can be speculated that Ambra1 deficiency makes
262 Ambra1-dependent synapses into silence (Figure 6). And, although Ambra1-dependent
263 synapses maintain silence, the fact that the reduction of glutamate-induced response is less
264 than that of synaptic responses such as eEPSC, mEPSC frequency and RRP size raise two
265 possibilities (Figure 6). Firstly, depletion of functional synaptic receptors that may be induced
266 by Ambra1 deficiency can lead to an increase in the number of extrasynaptic receptors. The
267 other possibility is that the *Ambra1* ^{gt/gt} neurons display the complete ablation of synaptic
268 release in Ambra1-dependent synapses. To elucidate the impairment of synaptic release and
269 its relationship to synaptic receptors, we recall our previous work (Sigler et al., 2017). The
270 number of functional synaptic glutamate receptors was reduced by approximately 40% in
271 Munc13-deficient synapses in which synaptic transmission from presynaptic terminal is
272 completely impaired. So, the difference between reduction ratios in synaptic parameters such
273 as the eEPSC size and mEPSC frequency, and glutamate induced responses in *Ambra1* ^{gt/gt}
274 can be attributed to the complete impairment of glutamate release. In order to support the two
275 hypotheses, it can be inferred that the Ambra1-dependent synapses accounts for about 50%
276 of the total synapses. Considering our data evaluating the expression levels of synaptic
277 receptors and scaffolding proteins (Figure S1), we highly appreciate the latter possibility. We
278 figured out that the most critical factor of E/I imbalance in *Ambra1* heterozygous brain is the
279 contribution of Ambra1 in the activity of glutamatergic synapses, regardless of autophagy. In
280 the end, we discovered that the novel function of Ambra1 in neuronal cells play an important
281 factor in ASD manifestation.

282 We conclude that *Ambra1*, localized specifically in neuronal cells, intrinsically triggers
283 excitatory synaptic activity, and that its sex-dimorphic expression of protein level modulates
284 the degree of glutamate release depending on sex (Dere et al., 2014). However, the
285 mechanism for the sex-dimorphic expression of *Ambra1* protein level is still an important piece
286 to be studied further. This sex-dimorphic reduction of synaptic transmission by *Ambra1*
287 haploinsufficiency might manifest female-specific phenotypes, such as autistic-like behaviors,
288 increased seizure propensity and aberrant gamma oscillations (Dere et al., 2014), which
289 provides us important insight on the neural substrate of E/I balance related with ASD and
290 epilepsy.

291

292 **Materials and methods**

293 Animals

294 *Ambra1* mutant mice were described previously¹⁹. Wild-type (WT, *Ambra1*^{+/+}) and
295 heterozygous *Ambra1*^{+/gt} (Het) littermates of both sexes with a >99% C57BL/6N genetic
296 background were obtained by interbreeding male *Ambra1*^{+/gt} and female WT C57BL/6N mice
297 and used for all experiments on postnatal animals. For neuronal cultures, *Ambra1*^{+/+},
298 *Ambra1*^{+/gt}, and *Ambra1*^{gt/gt} (KO) littermate embryos were obtained by interbreeding male and
299 female *Ambra1*^{+/gt} mice. All experiments were carried out in agreement with the guidelines for
300 the welfare of experimental animals issued by the Federal Government of Germany and Max
301 Planck Society.

302 Genotyping

303 Genomic DNA for genotyping was extracted from tail tips of 2-3 week-old offspring or embryos
304 using NucleoSpin Tissue kit (Machery-Nagel GmbH & Co. KG). WT and KO *Ambra1* alleles
305 and Y chromosomes of offspring were detected by polymerase chain reaction (PCR) of
306 genomic DNA. PCR analyses of *Ambra1* KO gene were performed as described previously²⁰
307 using GoTaq® G2 Flexi DNA polymerase (Promega). For *Ambra1* WT allele, GoTaq® G2 Flexi
308 DNA polymerase (Promega) with forward primer, 5'-AAC TGA ACC TGG GTT CTT TGA A-3'
309 and reverse primer 5'-GAA AAG CTC CCC ATC TTT TCT T-3' were used to generate a 0.5
310 kb fragment (95°C/5 min, 35 cycles with 95°C/30 s, 57°C/45 s, 72°C/105 s, and 72°C/ 10 min).
311 For sex determination of embryos, PCR analyses of Y chromosomes were performed using
312 GoTaq® G2 Flexi DNA polymerase, forward primer 5'-GGT GTG GTC CCG TGG TGA GAG-
313 3', and reverse primer 5'-GAG GCA ACT GCA GGC TGT AAA ATG-3' to generate a 270 bp
314 fragment (94°C/1 min, 33 cycles with 94°C/1 min, 63°C/30 s, 72°C/30 s, and 72°C/7 min). PCR

315 products were analyzed on a 1.5% agarose gel in Tris-Acetate-EDTA buffer, which were
316 stained with HDGreen® Plus Safe DNA Dye (Intas).

317 *mRNA expression of Ambra1 from data of Allen Brain Atlas*

318 Data of mRNA expression level in different brain regions were extracted from Allen Mouse
319 Brain Atlas (Figure 1a, <http://mouse.brain-map.org/>)^{51,52}. mRNA expression level in regions of
320 interests (ROIs) of in situ hybridization was calculated by multiplying expression density and
321 intensity.

322 *Histological and Immunohistochemical Analyses*

323 Mice were perfused transcardially with Ringer solution followed by 4% paraformaldehyde (PFA)
324 in 0.1 M phosphate buffer (PBS, pH=7.4). Brains were post-fixed at 4°C in 4% PFA in PBS for
325 2 h for X-galactosidase (X-gal) histochemical staining, or post-fixed overnight, followed by
326 cryo-protection in 30% sucrose solution in PBS and in liquid nitrogen for immunohistochemistry.

327 X-gal histochemical staining was performed with brains of 9 weeks old mice. Coronal brain
328 sections (50 µm) were cut using Leica VT1000S vibratome (Leica Biosystems) and incubated
329 overnight in the dark at 37°C in X-gal solution containing 5mM K₃[Fe(CN)₆]. 5mM K₄[Fe(CN)₆],
330 2mM MgCl₂ and 1.2 mg/mL 5-bromo-2-chloro-3 indoyl-b-D-galactopyranoside (X-gal) in PBS,
331 rinsed three times in PBS, and mounted with Aqua-Poly/mount (Polyscience). Digital images
332 were obtained using an Axiophot microscope (Carls Zeiss Microscopy GmbH).

333 *Ambra1* WT and Het female mouse brain were cut into coronal sections (30 µm) with Leica
334 CM1950 instrument (Leica Biosystems). Sections were blocked with 10% normal horse serum
335 (NHS) and 0.2% Triton-X-100 in PBS for 1 h at room temperature (RT). PBS with 5% NHS and
336 0.2% Triton-X-100 was also used for the primary and secondary antibody dilution. Incubation
337 of the primary antibodies was carried out at 4°C for 1-3 nights, followed by incubation of
338 secondary antibodies (1:500) for 2 h and DAPI (1:10,000, D9542, Sigma-Aldrich) in PBS for 5
339 min at RT. Washing was performed between every step and sections were mounted using
340 Aqua-Poly/mount. The following antibodies were used for immunochemistry: mouse anti-
341 β-gal (Z3781, Promega), chicken anti-NeuN (266006, Synaptic Systems), rabbit anti-IBA1
342 (019-19741, Wako), rabbit anti-Olig2 (AB9610, Chemicon), rabbit anti-GFAP (G5601,
343 Promega), guinea pig anti-Ctip 2 (325005, Synaptic Systems), mouse anti-GAD67 (MAB5406,
344 Chemicon), rabbit anti-PV (PV27, Swant), Alexa-Fluor 488 donkey anti-mouse IgG (A21202,
345 Invitrogen), Alexa-Fluor 488 donkey anti-chicken IgG (703-546-155, Jackson
346 ImmunoResearch), Alexa-Fluor 488 goat anti-chicken IgG (A-11039, Thermo Fisher Scientific),
347 Alexa-Fluor 555 goat anti-guinea pig IgG (A-21435, Thermo Fisher Scientific), Alexa-Fluor 555

348 goat anti-mouse IgG (A-21424, Thermo Fisher Scientific), Alexa-Fluor 594 goat anti-mouse
349 IgG (115-585-003, Jackson ImmunoResearch), Alexa-Fluor 594 donkey anti-rabbit IgG (A-
350 21207, Invitrogen) and Alexa-Fluor 633 goat anti-rabbit IgG (A-21071, Thermo Fisher
351 Scientific). Leica TCS SP5 confocal microscope (Leica Biosystems) was used to scan
352 anatomically matched sections using 0.5 μ m z-step and a 20x objective lens. For counting cell
353 numbers, the dorsal part of hippocampus (Bregma -1.34 to -2.54 mm posterior) was used
354 bilaterally in each animal (12-14 hippocampi per 1-2 animal). Image stacks were further
355 processed by Image J and quantification of CTIP2+, GAD67+ and PV+ were done using Imaris
356 7.5.1 and manually. Cell density was obtained by dividing the number of each cell type by the
357 total volume of hippocampal region in mm³.

358 Protein Extraction and Measurement

359 Cortices of 6-weeks old mice and hippocampi of 4-weeks old mice were dissected in cold 0.32
360 M sucrose solution with protease inhibitors (0.1 μ M Aprotinin, 50 μ M Leupeptin, 0.2 mM PMSF)
361 and homogenized using glass-teflon homogenizer (900 rpm, 10 strokes). Cortical homognates
362 of male WT and female WT and Het mice at 6 weeks of age were used for purification of
363 synaptic membrane proteins (Fig. 1f). All centrifugations were performed with Beckman TL-
364 100 Ultracentrifuge (Beckman Coulter) at 4°C. Cortical homogenates were layered on a
365 discontinuous gradient of 0.85 M, 1.0 M, and 1.2 M sucrose solutions. After centrifugation at
366 82,500 g for 2 h, the supernatant above 0.85 M sucrose layer and the pellet were kept as
367 soluble fraction (S) and mitochondria-enriched fraction (P2D), respectively. The interface
368 fractions between 0.32 M and 0.85 M sucrose, between 0.85 M and 1.0 M sucrose, and
369 between 1.0 M and 1.2 M were collected as myelin-enriched fraction (P2A), ER-Golgi-enriched
370 Fraction (P2B), and synaptosome fraction (P2C), respectively. The P2C fraction was diluted
371 with 0.32 M sucrose solution with protease inhibitors and centrifuged at 100,000 g for 20 min.
372 After centrifugation, the resulting pellet was resuspended in 2.5 mL of 6 mM Tris-Cl, pH 8 and
373 incubated on ice for 45 min for osmotic shock. After centrifugation at 32,800 g for 20 min, the
374 supernatants were collected as synaptic cytoplasm and crude synaptic vesicle (SC/CSV)
375 fractions, and the pellets were resuspended as crude synaptic membrane (CSM) fraction with
376 3 mL of 0.32 M sucrose solution with protease inhibitors. CSM fractions were applied to a
377 discontinuous gradient of 0.85 M, 1.0 M, and 1.2 M sucrose solutions and centrifuged at 82,500
378 g for 2 h. The interface fraction between 1.0 M and 1.2 M sucrose was harvested as pure
379 synaptic membrane fraction (SM) and diluted in 0.32 M Sucrose solution with protease
380 inhibitors, followed by centrifugation at 100,000 g for 20 min. The resulting pellet was re-
381 suspended in 500 μ L of 6 mM Tris-Cl pH 8.0. Purified fractions were stored at -80°C. Protein

382 concentrations in various samples were measured using Bradford method (Bio-Rad) according
383 to the manufacturer's instructions.

384 **Western Blotting**

385 SDS-PAGE and protein transfer to nitrocellulose membranes were performed according to
386 standard procedures.^{53,54} After transfer, the membranes were washed with ultra-pure water
387 and incubated with Memcode Reversible Protein Stain Kit (Thermo Fisher Scientific) according
388 to the manufacturers' protocol. Membranes were washed and incubated in blocking buffer (5%
389 milk powder in Tris-based saline with 0.05 % Tween-20, TBST) for 1 h at RT. followed by
390 incubation with primary antibodies diluted at 1:1000 in blocking buffer for 3 h at RT. Membranes
391 were then incubated with primary antibodies (1:1000) and secondary antibodies (1:5000) with
392 washing three times with TBST for 15 min each between. Protein signals were detected with
393 Odyssey Infrared Imaging System (LI-COR Biosciences GmbH) and quantified using the
394 Image-Studio Software (Odyssey System; LI-COR Biosciences GmbH) with normalization to
395 total protein assessed by Memcode staining. The following antibodies were used for Western
396 blotting: mouse anti-PSD95 (ab2723, Abcam), mouse anti-Gephyrin (147111, Synaptic
397 Systems), rabbit anti-GluR1 (PC246, Calbiochem), rabbit anti-GluR2 (182103, Synaptic
398 Systems), mouse anti-NMDAR1 (114011, Synaptic Systems), rabbit anti-GuR6/7 (04-921,
399 Millipore), rabbit anti-GABA_AR α 1 (Ab5592, Chemicon GmbH), rabbit anti-GABA_AR γ 2 (Ab82970,
400 Abcam), rabbit anti-vGluT1 (135302, Synaptic Systems), mouse anti- β -Tubulin (T4026,
401 Sigma-Aldrich), IRDye680-anti-mouse IgG (926-68070, LI-COR Biosciences GmbH),
402 IRDye800-anti-rabbit IgG (926-32211, LI-COR Biosciences GmbH).

403 **Pentylenetetrazol (PTZ)-Induced Seizures**

404 Seizure activity was induced in awake 12-13 weeks-old Ambra1 WT and Het mice of both
405 sexes by a single intraperitoneal (i.p.) injection of 50 mg of Pentylenetetrazol (PTZ; P6500,
406 Sigma-Aldrich) per 1 kg of body weight. After injection, mice were observed closely for 30 min
407 in a small clear home cage. Four phases of behavioral response to PTZ injection were defined
408 as follows: (1) Hypoactivity; decrease in mobility until the animal arrests in a crouched posture.
409 (2) Partial clonus (PC), clonic seizure activity in face, head, and forelimbs. (3) Generalized
410 clonus (GC); sudden loss of upright posture, whole body clonus including all four limbs and tail,
411 rearing and autonomic signs. (4) Tonic-clonic (TC) (maximal) seizure; generalized seizure with
412 tonic hind-limb extension followed by death. The latency to GC and the seizure score, which
413 is calculated from the latencies to PC, GC, and TC in seconds by equation [Seizure score =
414 1000 / (0.2 * PC latency + 0.3 * GC latency + 0.5 * TC latency)] were used as measures⁵⁵.

415 **Electrophysiological recordings**

416 Four weeks old WT and *Ambra1* Het mice were anesthetized with Isoflurane and decapitated.
417 During the entire procedure, carbogen gas (95% oxygen and 5% carbon dioxide) keeps
418 applied in solutions. The whole brain was immediately transferred to cold slicing solution (230
419 mM Sucrose, 26 mM NaHCO₃, 1 mM KH₂PO₄, 2 mM KCl, 2 mM MgCl₂·6H₂O, 10 mM Glucose,
420 0.5 mM CaCl₂). To get hippocampal slices for evoke field excitatory postsynaptic potentials
421 (fEPSP) recording, hippocampi were isolated carefully and cut transversally at 300 µm
422 thickness using a McILWAIN tissue chopper (Molecular Devices, LLC). For acute brain slices,
423 sagittal sections at 5° angle tilted to the midline with 300 µm thickness were obtained inside
424 the same slicing solution at 4°C using Leica VT1200S vibrotome (Leica Biosystems). Slices
425 were immediately transferred to a chamber filled with artificial cerebrospinal fluid (ACSF; 120
426 mM NaCl, 26 mM NaHCO₃, 1 mM KH₂PO₄, 2 mM KCl, 2 mM MgCl₂·6H₂O, 10 mM Glucose, 2
427 mM CaCl₂) at 37°C for 1h 40min for hippocampal slices and at 37°C for 20 min for acute brain
428 slices. After recovery, slices were kept at RT.
429 For fEPSP measurement, the hippocampal slices were placed in interface recording chamber
430 (Harvard Apparatus) with continuous flow of carbogen-supplied ACSF at 30°C. An electric
431 stimulation was applied with 100 µs duration time by concentric metal bipolar electrode (FHC)
432 on the *Stratum radiatum* of Schaffer collaterals. Recording electrode (2-3 MΩ) was pulled from
433 thin-walled borosilicate glass capillaries, filled with ACSF, and positioned on the *Stratum*
434 *radiatum* of CA1 area.
435 For kainite-induced gamma oscillation recording, acute brain slices were placed on interface
436 recording chamber with application of ACSF at 33°C. Recording electrode (2-3 MΩ), filled with
437 ACSF, was placed in the CA3 pyramidal layer of hippocampus. For each slice, baseline field
438 potentials were recorded for 30 min in ACSF, followed by recording of oscillatory field potentials
439 in gamma-range induced by 100 nM kainic acid (BN0281, BIOTREND Chemikalien GmbH) in
440 ACSF for 30 min. After this recording phase, the electrode was slightly re-positioned to acquire
441 the maximum power of gamma oscillation for another 10 min. Recordings were acquired by
442 Multiclamp 700B amplifier and Digidata 1440A (Molecular Devices, LLC.) and data were
443 analyzed using AxographX (Axograph), as previously described⁵⁶.
444 For whole-cell recordings, the somata of hippocampal CA1 pyramidal neurons in acute brain
445 slice were whole-cell voltage clamped at -70 mV by recording electrode (2.5-3.5 MΩ)
446 containing internal solution with 100 mM KCl, 50 mM K-gluconate, 10 mM HEPES, 4 mM ATP-
447 Mg, 0.3 mM GTP-Na, 0.1 mM EGTA, 0.4% biocytin, pH 7.4, 300 mOsm. The external solution
448 was carbogen-saturated ACSF. Miniature excitatory and inhibitory post-synaptic currents
449 (mEPSCs/mIPSCs) were recorded in the presence of 1 µM TTX, mixed with 10 µM bicuculline
450 methiodide for measuring mEPSCs or with 10 µM NBQX for measuring mIPSCs with washing

451 with 1 μ M TTX for 15 mins between. An EPC-10 amplifier with Patchmaster v2X80 software
452 was used for data acquisition (HEKA/Harvard Bioscience). Subsequently, slices were fixed
453 using 4% PFA in PBS for two hours at RT and washed by PBS.

454 *Immunohistochemistry of Biocytin-filled Neurons*

455 After being washed in PBS, blocked and permeabilized for 1h with blocking solution (5% NGS
456 and 0.5% Triton X-100 in PBS), fixed brain slices obtained from patching were stained with
457 Alexa-Fluor-555-labeled streptavidin (1:1000; S32355, Thermo Fisher Scientific.) and DAPI
458 (1:10,000) in blocking solution. After washing, the slices were mounted on glass slides and
459 covered with cover slips in Aqua-Poly/Mount. CA1 pyramidal neurons in hippocampus were
460 scanned using a Leica SP5 confocal microscope with 100 x/1.44 NA oil objective at 0.126 μ m
461 z-intervals. The basal and apical part of pyramidal neurons 3D Gaussian-filtered (σ_x, y 0.7, σ_z
462 0.7,), using custom-written macros to handle the large data sets. Only cells with a pyramidal
463 shape and a location in CA1 were used for further analysis.

464 *In Utero Electroporation and Immunohistochemistry for Sholl Analysis*

465 E14.5 mouse embryos from WT mothers bred with Het males were subjected to IUE (permit
466 number 33.19-42502-04-13/1052), as previously described^{57,58}. DNA solution with pFUGW
467 (0.1 mg/mL) and pCX::myrVENUS (0.1 mg/mL) for the myrVenus construct^{59,60} were used to
468 sparsely label CA1 pyramidal neurons in hippocampus.

469 *In utero* electroporated mice were perfused, and brains were post-fixed and cryo-protected
470 (15%-30% sucrose in PBS) at P28. Coronal brain sections (230 μ m thickness) at -1.06 mm to
471 -2.46 mm from Bregma were collected using a Leica VT 1000S vibrotome. For
472 immunofluorescence staining, PFA was quenched by 1 mg/mL NaBH₄ in PBS for 5 min
473 followed byh thorough washing in PBS. Brain sections were incubated in blocking solution (5%
474 normal goat serum (NGS) and 0.5 % Triton-X-100 in PBS) for 1 h at RT followed by incubation
475 in 0.2% Tween-20 and 10 μ g/mL heparin in PBS for 1.5 h to improve the penetration of
476 antibody in thick brain sections. The blocking solution was used for diluting primary and
477 secondary antibodies (1:1000 dilution). The sections were incubated with polyclonal rabbit anti-
478 GFP antibody (598, MBL) for 4 days at 4°C and with Alexa-Fluor (AF) 488 goat anti-rabbit IgG
479 (R37116, Thermo Fisher Scientific) overnight at RT followed by DAPI staining (1:10,000) and
480 mounted on slides. Images of CA1 pyramidal neurons in hippocampus were acquired with 1.02
481 μ m z-steps by Leica SP2 confocal microscope (Leica Biosystems) and oil-immersion 20x
482 objective.

483 *Analysis of Neuron Morphology using NeuronStudio*

484 For segmentation of entire dendritic trees and subsequent mushroom spine analysis, we used
485 NeuronStudio (CNIC, Mount Sinai School of Medicine, New York, NY, USA)⁶¹. After
486 reconstructing the dendritic trees, 3D Sholl analysis from this program was performed to
487 acquire the accumulative dendritic length in every 10 μ m step from the center of soma.⁶²
488 Mushroom spines were automatically detected along the reconstructed dendritic trees using
489 the NeuronStudio segmentation algorithm by keeping the suggested parameters^{48,61} (Head
490 diameter of mushroom spines: 0.35 μ m) and the numbers of mushroom spines were counted
491 every 10 μ m from the center of soma.

492 Autaptic Neuron Culture and Electrophysiology

493 Autaptic cultures of cortical glutamatergic neurons from hippocampi from E14.5 embryonic
494 brains or striatum of P0 postnatal brains were prepared according to a previously published
495 protocol⁶³ with slight modifications. 3,000 to 3,500 cells were plated on 35 mm² coverslips with
496 astrocyte islands in Neurobasal-A Medium with supplements.

497 Autaptic neurons were analyzed electrophysiologically as described previously⁶⁴ at day in vitro
498 (DIV) 10-16. Autaptic neurons were whole-cell voltage clamped at -70 mV with a
499 MultiClamp700B amplifier (Axon Instruments, Molecular Devices) under the control of the
500 Clampex program 10.1 (Molecular Devices). The internal solution for recording autaptic
501 neurons consisted of 136 mM KCl, 17.8 mM HEPES, 1 mM EGTA, 4.6 mM MgCl₂, 4 mM
502 NaATP, 0.3 mM Na₂GTP, 15 mM creatine phosphate, and 5 units/mL phospho-creatine kinase
503 (315-320 mosmol/L), pH7.4. Extracellular solution contained 140 mM NaCl, 2.4 mM KCl, 10
504 mM HEPES, 10 mM glucose, 4 mM CaCl₂, and 4 mM MgCl₂ (320 mosmol/L), pH 7.3. All
505 chemicals were purchased from Sigma-Aldrich (Sigma-Aldrich) unless mentioned otherwise.

506 Evoked post synaptic currents (PSCs) were measured by depolarization of neurons from -70
507 to 0 mV for 2 ms. Readily releasable vesicle pool size (RRP) was recorded by measuring PSC
508 in response to application of 0.5 M hypertonic sucrose in extracellular solution. P_{vr} was
509 calculated by dividing the charge transfer during an action potential-evoked response by the
510 charge transfer measured during a response to hypertonic solution. Additionally, EPSC
511 amplitudes were measured after application of 50 stimuli at 10 Hz to assess short-term
512 depression. Glutamate-induced response was measured by focal application of 100 μ M
513 glutamic acid (Sigma) in order to study the cell surface expression of glutamate receptor.
514 mEPSCs were recorded in the presence of 300 mM TTX (Tocris). Given that three genotypes
515 of identical sex are difficult to obtain in the same litters, the data were normalized to WT mean
516 values obtained in several sets of experiments.

517 Immunofluorescent staining and analysis of pre- and post-synaptic puncta in autaptic neurons

518 At DIV 18-23 from two independent cell preparation, autaptic cultured neurons were fixed in a
519 solution containing 4% PFA/4% sucrose in PBS, pH7.4, for 20 min. After washing with PBS for
520 3 times, cells were incubated in blocking solution containing 0.3% Triton-X-100, 10% NGS and
521 0.1% fish skin gelatin (Sigma) in PBS for 20 min. Neurons were incubated with primary
522 antibodies against vGluT1 (1:1000, rabbit polyclonal, 135303, Synaptic Systems), PSD95
523 (1:200, mouse monoclonal, ab2723, Abcam), and MAP2 (1:500, chicken polyclonal, NB300-
524 213, Novus biologicals) diluted in blocking solution for overnight at 4°C. After repetitive
525 washing with PBS, neurons were incubated with secondary antibodies diluted in blocking
526 solution, including Alexa-Fluor 488 goat anti-chicken IgG (1:1000, A-21441, Invitrogen), Alexa-
527 Fluor 555 goat anti-rabbit IgG (1:1000, A-32732, Invitrogen) and Alexa-Fluor 633 goat anti-
528 mouse IgG (1:1000, A-21052, Invitrogen) for 2 hrs at RT, followed by another rounds of
529 washing. After DAPI staining, coverslips were mounted on slides.

530 Single autaptic neurons were imaged by Leica SP2 confocal microscope using 40x objective
531 (resolution: 1024 x 1024 pixels) with 1 µm z-step and analyzed using Image J software, as
532 referenced from previous publication⁵⁶. Briefly, for the quantification of pre- and post-syanptic
533 puncta, the fluorescent signals of vGlut and PSD95 were thresholded and binarized followed
534 by being watersheded. The number of their puncta was analyzed using 'Analyze
535 particle' option. For the colocalization of pre- and post-synaptic marker, the Manders' overlap
536 coefficient was calculated by Intensity Correlation Analysis plugin.

537 Statistical Analysis

538 All data were analyzed separately for males and females. Statistical methods are described in
539 figure legends. All statistics were performed with Excel (Microsoft), GraphPad Prism 5 software
540 (GraphPad software) and SPSS 17 (SPSS Inc.). Data are presented as mean±S.E.M., and p-
541 values <0.05 were considered as indicating a significant difference.

542

543 **Acknowledgment**

544 We thank F. Benseler, for valuable advice and excellent technical support. We are grateful to
545 the staffs at the animal facility of the Max Planck Institute for Multidisciplinary Sciences for
546 mouse husbandry.

547

548

549 **Additional information**

550 **Funding**

Funder	Grant reference number	Author
European Commission	H2020, Comorbidity and Synapse Biology in Clinically Overlapping Psychiatric Disorders, Project ID 667301	Jeongseop Rhee, Nils Brose
Max Planck Society	open access funding	Jeongseop Rhee, Nils Brose, Hannelore Ehrenreich
DFG	CNMPB	Hannelore Ehrenreich
EXTRABRAIN	EU-FP7	Hannelore Ehrenreich
Niedersachsen-Research Network on Neuroinfectiology (N-RENNT)	open access funding	Hannelore Ehrenreich
European Union's Seventh Framework Program (FP7/2007–2013), the EFPIA companies and Autism Speaks	EU-AIMS	Hannelore Ehrenreich

551 The funders had no role in study design, data collection and interpretation, or the decision to
552 submit the work for publication.

553

554 **Author contributions**

555 Conceptualization: JSR and AJ; Methodology: JSR, AJ, BA, HJR, AS, HE, IH, MS, HK;
556 Investigation: JSR, AJ, BA, HJR, HE, IH, MS, HK; Writing (Original draft): JS and AJ; Writing
557 (review & editing): JS, AJ and NB; Funding acquisition: JSR, NB and HE; Resources: JSR, NB
558 and HE; Supervision: JSR

559 Nils Brose (NB) is under competing interests for being a reviewing editor of this journal. Other
560 authors declare that there is no competing of interest.

561

562 **Ethics**

563 All experiments were carried out in agreement with the guidelines for the welfare of
564 experimental animals issued by the Federal Government of Germany and Max Planck Society.

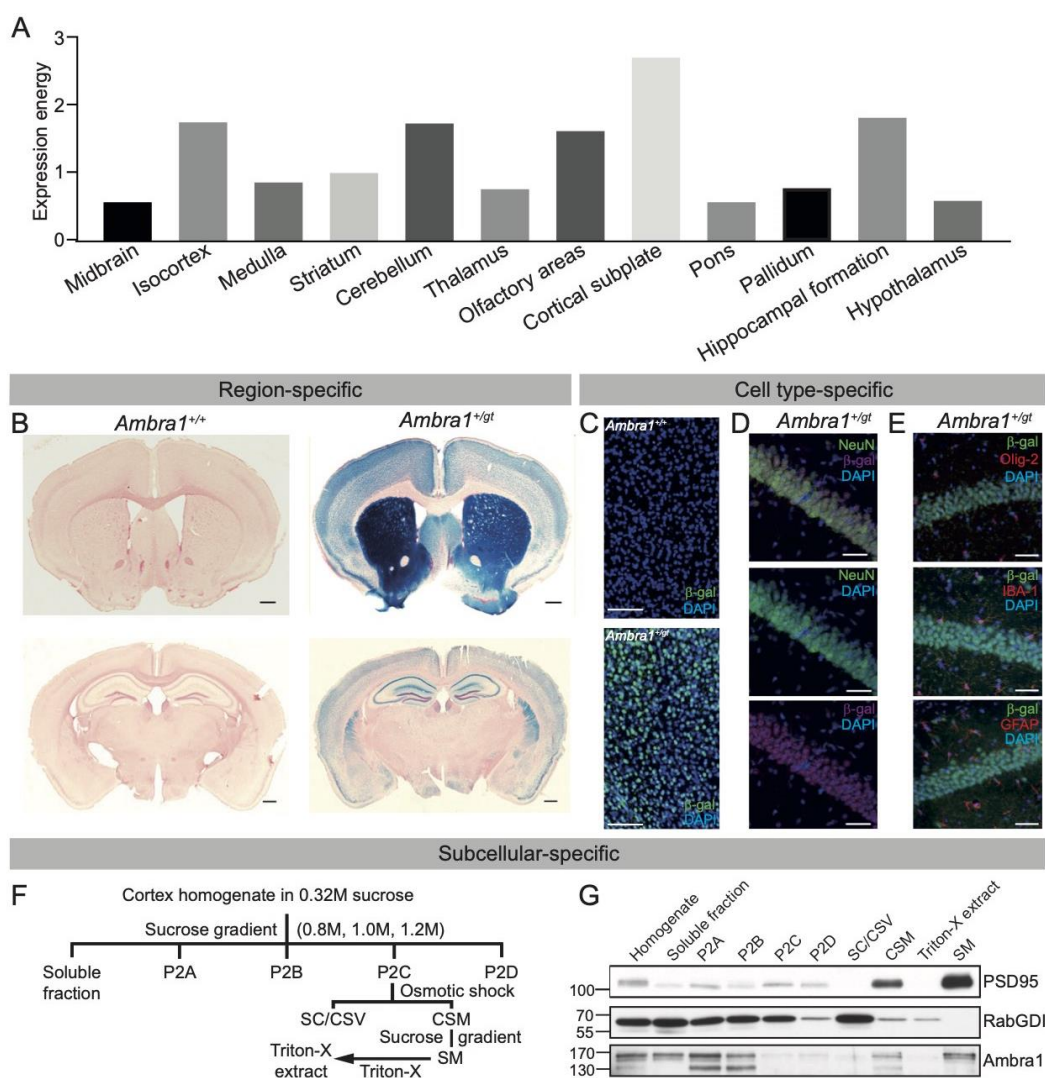
565

566 **Data availability**

567 Most of data generated or analyzed during this study are included in the manuscript and
568 supporting files.

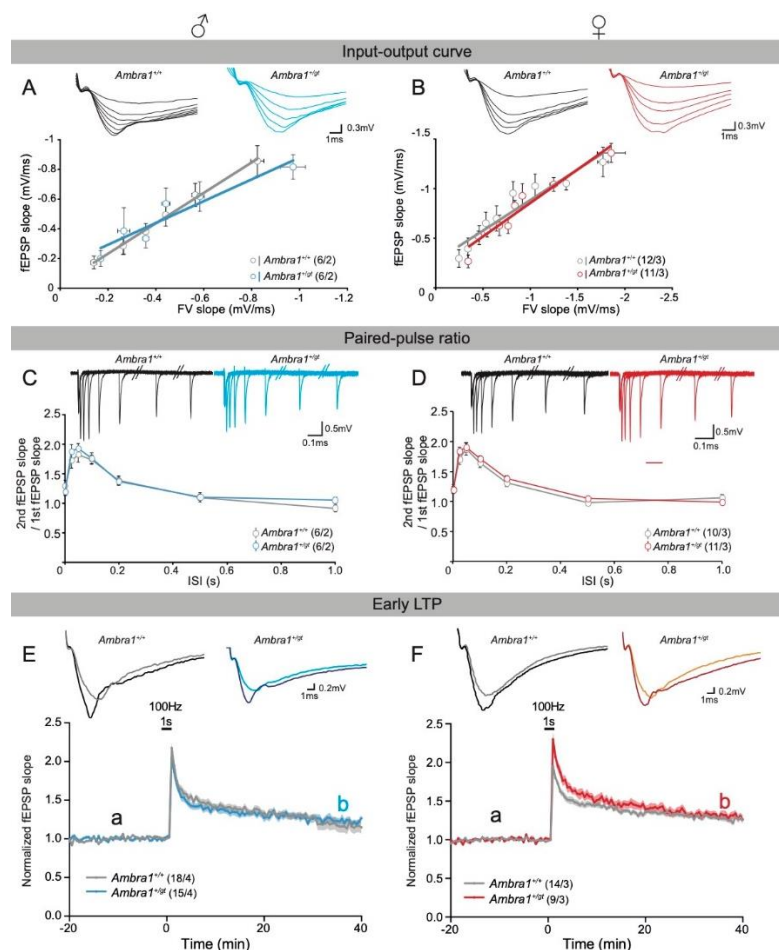
569

570 **Figure**



571
572 **Figure 1: Region-, cell type- and subcellular specific location of Ambra1 protein in the**
573 **brain**

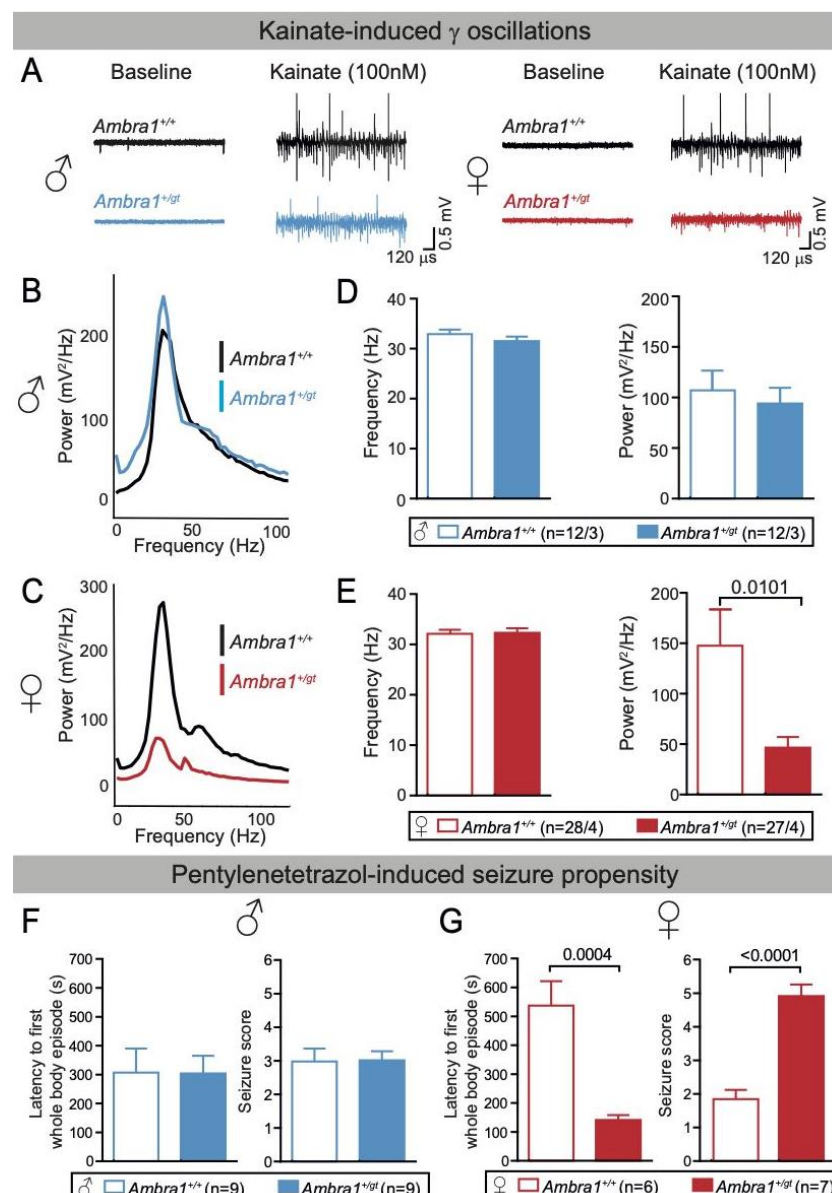
574 **A** Expression level of Ambra1 mRNA in different brain regions of a mouse (n=1). **B** X-
575 galactosidase staining in coronal brain section of *Ambra1^{+/+}* and *Ambra1^{+/gt}* mice. Scale bar,
576 100 μ m. **C** Immunofluorescence staining of β -galactosidase (β -gal). **D, E** Co-staining of β -gal
577 with different cellular markers, including neuronal marker, NeuN (**D**) or glial markers, Olig-2,
578 IBA-1 and GFAP (**E**) in hippocampal CA1 pyramidal region of *Ambra1^{+/gt}* mouse. Scale bar, 40
579 μ m. **F** Schematic representation of the subcellular fractionation step. P2A, Myelin-enriched
580 fraction; P2B, ER/Golgi-enriched fraction; P2C, Synaptosome fraction; P2D, Nucleus- and
581 mitochondria-enriched fraction; SC, Synaptic cytoplasm; CSV, Crude synaptic vesicles; CSM,
582 Crude synaptic membrane; SM, Pure Synaptic Membrane Fractions. **G** Western blots of
583 PSD95, RabGDI and Ambra1 proteins in subcellular fractions of *Ambra1^{+/+}* mouse cerebral
584 cortex. PSD95 and RabGDI were used for verification of purification of SM fraction.



585

586 **Figure 2: Activity-dependent synaptic transmission and short- and long-term synaptic**
 587 **plasticity of hippocampal CA1**

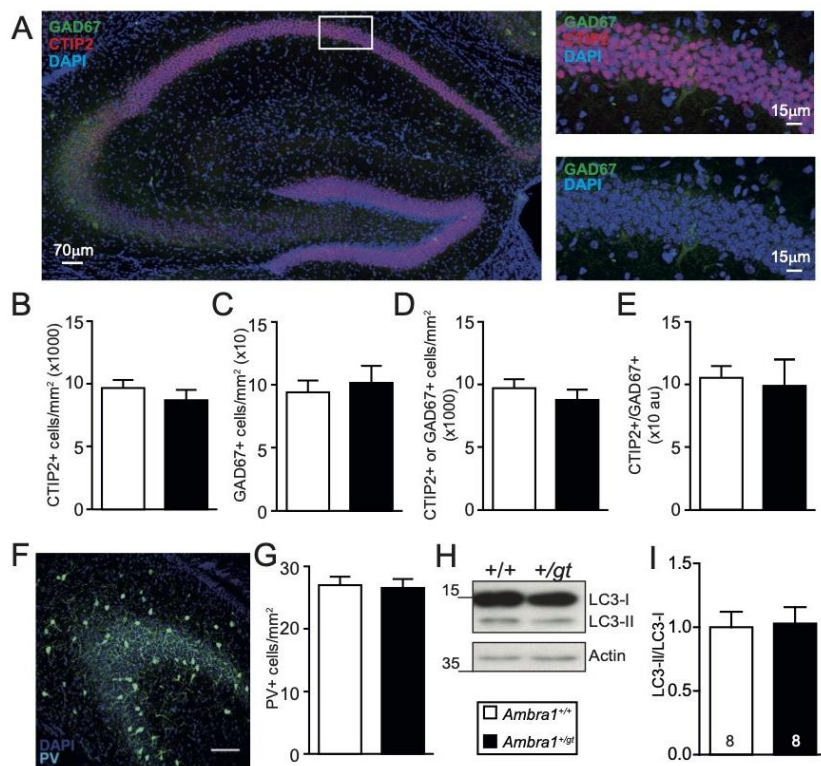
588 Left panel contains data from male mice, while right panel represents data from female mice.
 589 Field excitatory postsynaptic potential (fEPSP) slope was recorded in the *Striatum Radiatum*
 590 of CA1 upon Schaffer-Collateral stimulation in acute hippocampal slice. **A, B** Input-output
 591 curve from *Ambra1^{+/+}* (black) and *Ambra1^{+gt}* (color) mice in both sexes. fEPSP slopes were
 592 measured after increasing the stimulus intensity and plotted along their fiber volley (FV) slopes.
 593 **C, D** Paired-pulse ratio curve from two genotypes in both sexes. Ratios of 2nd and 1st fEPSP
 594 slope (Paired-pulse ratio) after two stimuli within different time intervals (Interstimulus interval,
 595 ISI) were plotted along their respective intervals. Representative traces were shown within
 596 graphs. **E, F** Early-phase long-term potentiation (E-LTP) from two genotypes in both sexes.
 597 fEPSP slopes after stimuli every 30 second were normalized to baseline and plotted along
 598 time. After 20 minutes of baseline, a high frequency stimulation (100 Hz for 1 sec) was given
 599 to induce potentiation. Representative traces are shown within graphs (light color: baseline,
 600 dark color: potentiation). N numbers are written next to the legend within the graphs and shown
 601 as slice number/animal number. Mean \pm S.E.M. are presented in line and area and statistical
 602 difference was defined by p-value between genotypes from Repeated-Measures of ANOVA.



603

604 **Figure 3: Perturbed γ -power and seizure propensity only in Ambra1^{+/gt} females but not**
605 **in males**

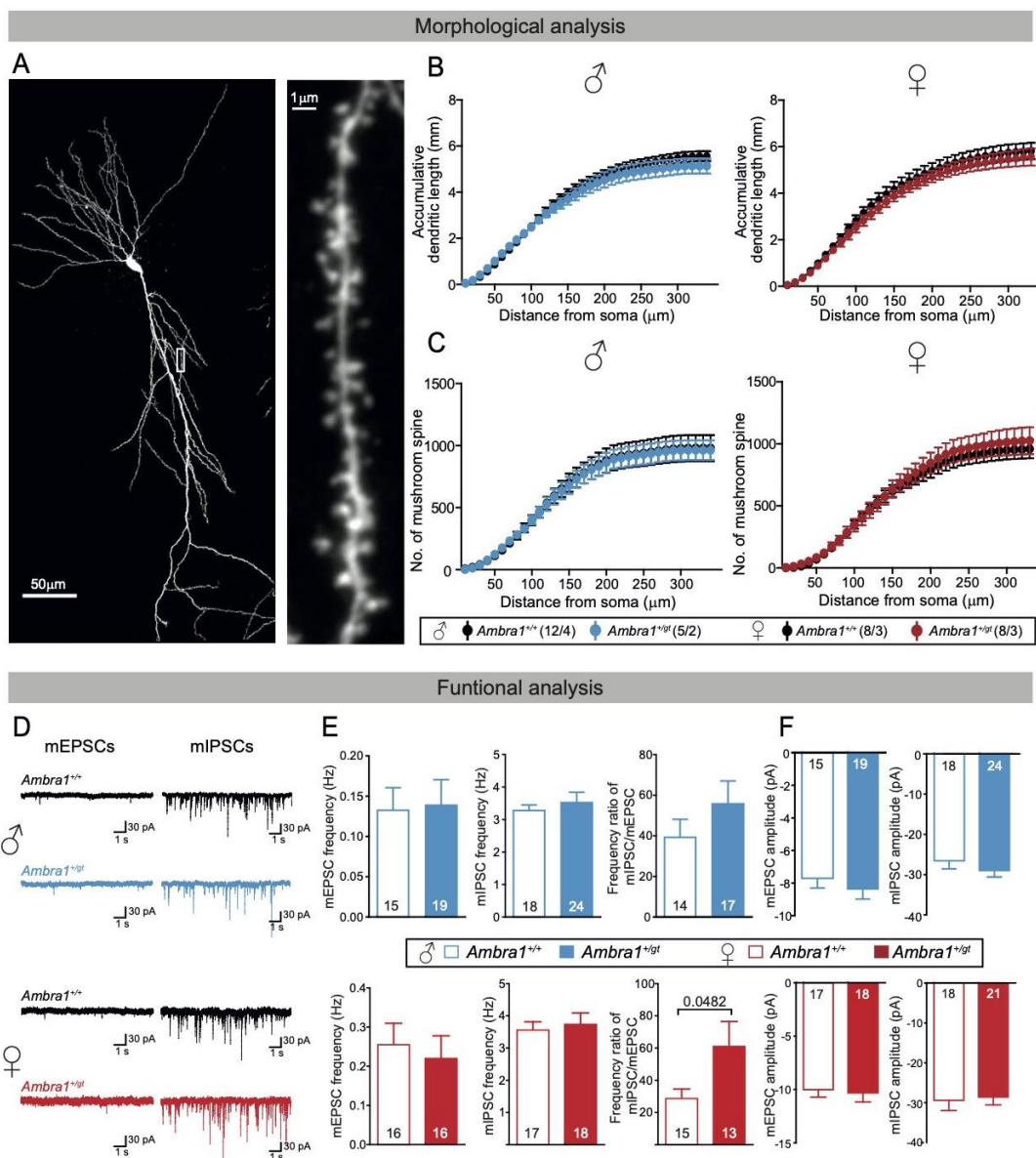
606 **A** Representative traces of γ -oscillations before and during being induced by 100 nM kainate
607 in hippocampal CA3 pyramidal layer of acute brain slices in Ambra1^{+/+} and Ambra1^{+/gt} male
608 and female mice. **B, C** Representative power spectrums of gamma oscillations are shown. **D,**
609 **E** Quantifications of the frequency of maximum power and average power within gamma range
610 (25-45 Hz) at 4 weeks old. **F, G** Latency to first whole-body episode and seizure score were
611 measured during observation after injection of pentylenetetrazol (50mg/kg) in 12-13 weeks old
612 mice. The bar graphs are presented as mean \pm S.E.M and slice number/animal number or
613 animal numbers of each group are noted next to the legends. Statistical analysis between
614 Ambra1^{+/+} and Ambra1^{+/gt} was performed by two-tailed unpaired t-test with significance level p
615 < 0.05 .



616

617 **Figure 4: Comparable neuronal numbers and autophagic activity in the brains of**
618 ***Ambra1*^{+/+} and *Ambra1*^{+/gt} mice**

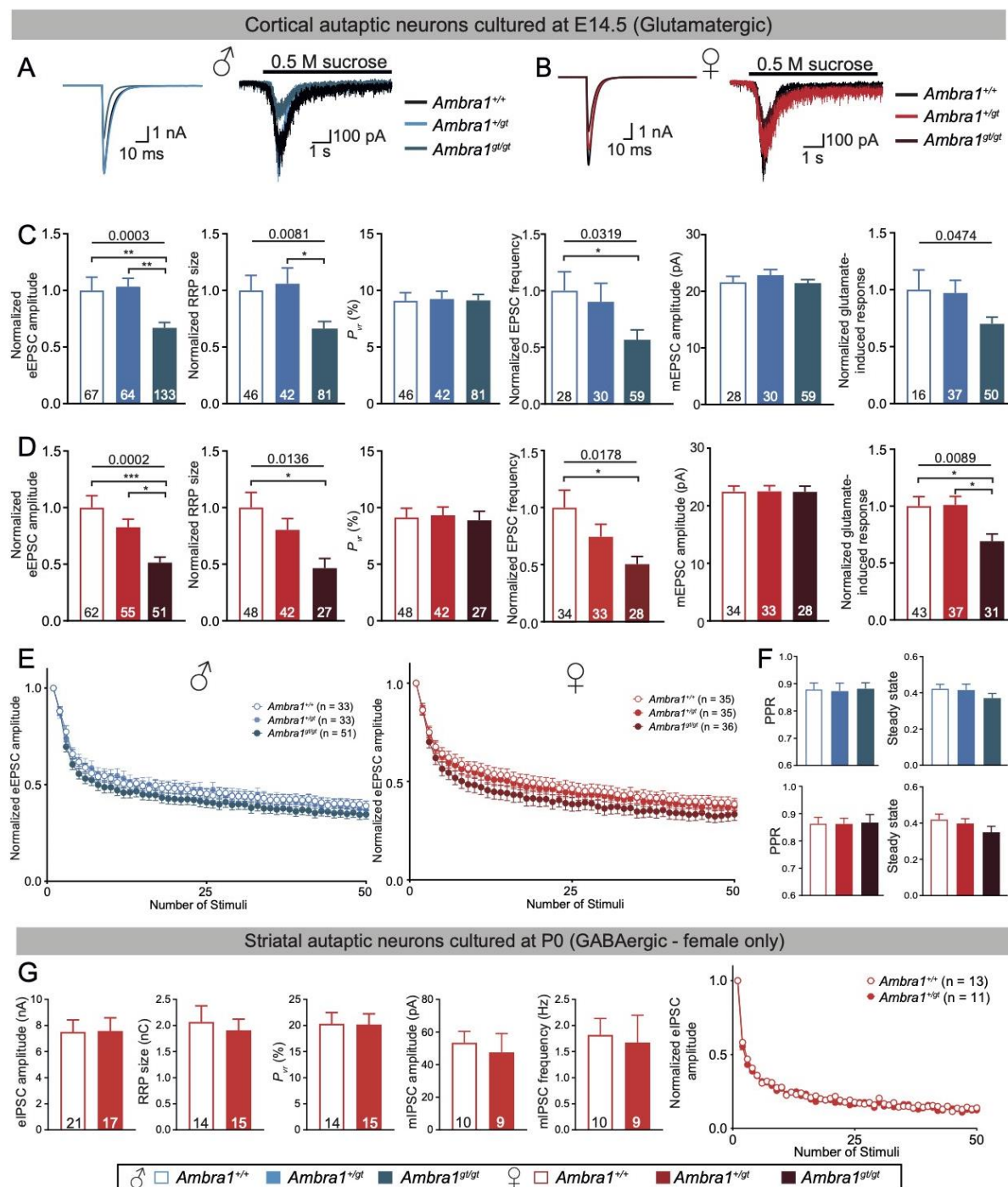
619 **A** Example images of hippocampal CA1 region immunostained with anti-CTIP2 and anti-
620 GAD67 antibodies. **B-E** The quantifications of the density of CTIP2+ (B), GAD67+ (C), sum of
621 CTIP2+ and GAD67+ neurons (D) and ratio of CTIP2+ and GAD67+ neurons (E) in *Ambra1*^{+/+}
622 and *Ambra1*^{+/gt} mouse hippocampus. **F** Example images of hippocampal CA3 region
623 immunostained with an anti-PV antibody. 4 weeks old wild type mouse was used. **G** The
624 quantifications of PV+ neurons in *Ambra1*^{+/+} and *Ambra1*^{+/gt} mouse hippocampus. 13-15
625 sections in 1-2 animals were used for analysis per group. **H** Sample picture of LC3 Western
626 Blot between cortical homogenates of both genotypes (n=8 for each group) in female mice.
627 The data was normalized to the average value of wild-type group. **I** Comparison of LC3-II and
628 LC3-I intensities between two genotypes. The bar graphs represent mean \pm S.E.M and
629 statistical analysis was performed by two-tailed unpaired t-test with significance level $p < 0.05$.
630



631

632 **Figure 5: Imbalance of excitatory and inhibitory inputs upon *Ambra1* heterozygous
633 mutation in female-specific manner**

634 **A** Example images of CA1 pyramidal neuron. **B, C** Accumulative dendritic length (**B**) and
635 number of mushroom-shaped spines (**C**) were plotted along the distance from soma. Numbers
636 written in brackets next to the legends represent neuron numbers/animal numbers. **D**
637 Representative traces of mEPSC with 10 μM bicuculline and mIPSC with 10 μM NBQX from
638 both genotypes. **E, F** The frequencies of mEPSC and mIPSC, frequency ratio of
639 mIPSC/mEPSC (**E**), and amplitudes of mEPSC and mIPSC (**F**) in two genotypes of male
640 (upper) and female (lower) mice. Numbers written within bars represent neuron numbers
641 acquired from 4-5 animals per group. All experiments were performed at 4 weeks old. The
642 spots and bars represent mean ± S.E.M and statistical analysis was performed by two-way
643 ANOVA (**B, C**) and two-tailed unpaired t-test (**E, F**) with significance level $p < 0.05$.



644 **Figure 6: Aberrant synaptic transmission in the absence of *Ambra1* gene, regardless of
645 sex**

646 **A, B** Sample traces of eEPSC and 0.5 M sucrose-induced response from glutamatergic
647 autaptic neurons from E14.5 hippocampal-like embryonic brain of *Ambra1^{+/+}*, *Ambra1^{+gt}* and
648 *Ambra1^{gt/gt}* in males (**A**) and females (**B**). **C, D** The bar graphs of normalized eEPSC amplitude,
649 normalized RRP size, P_{vr} , normalized mEPSC frequency, mEPSC amplitude and 100 μ M
650 glutamate-induced response between three genotypes in males (**C**) and females (**D**),
651 separately. **E** Short-term synaptic depression was monitored after application of 50 stimuli at
652

653 10 Hz. **F** Comparison of normalized eEPSC amplitude acquired from 2nd stimuli (Paired pulse
654 ratio (PPR), left) and averaged during the steady state (36-40th stimuli, right) from 10 Hz
655 stimulation experiment (**E**). **G** The bar graphs of eIPSC amplitude, RRP size, P_{vr} and
656 amplitudes and frequency of mIPSC and a dot graph of short-term synaptic depression by 50
657 stimuli at 10 Hz in GABAergic autaptic neurons from P0 striatum of *Ambra1^{+/+}* and *Ambra1^{+gt}*
658 females. Neuron numbers of each group are written within the bar or next to the legends from
659 2-4 independent experiments and the bars and dots in graphs are presented as mean \pm S.E.M.
660 Statistical analysis of bar graphs from three groups (**C, D, and F**) was performed by one-way
661 ANOVA followed by Bonferroni or Tukey post-hoc test showing significance as asterisk (*,
662 $p \leq 0.05$; **, $p \leq 0.01$; ***, $p \leq 0.001$) and from two groups (**G**) by two-tailed unpaired t-test with
663 significance below 0.05. Short-term synaptic depression (**E, G**) was analyzed by Repeated
664 Measures of ANOVA.

665

666 **References**

667 Association AP. 2013. Diagnostic and Statistical Manual of Mental Disorders, Diagnostic and
668 Statistical Manual of Mental Disorders. American Psychiatric Association.
669 doi:10.1176/appi.books.9780890425596.x00DiagnosticClassification

670 Baron-Cohen S, Lombardo M V., Auyeung B, Ashwin E, Chakrabarti B, Knickmeyer R. 2011.
671 Why Are Autism Spectrum Conditions More Prevalent in Males? *PLoS Biol* **9**:e1001081.
672 doi:10.1371/journal.pbio.1001081

673 Bermejo MK, Milenkovic M, Salahpour A, Ramsey AJ. 2014. Preparation of Synaptic Plasma
674 Membrane and Postsynaptic Density Proteins Using a Discontinuous Sucrose Gradient.
675 *J Vis Exp* 51896. doi:10.3791/51896

676 Bolton PF, Carcaci-Rathwell I, Hutton J, Goode S, Howlin P, Rutter M. 2011. Epilepsy in autism:
677 features and correlates. *Br J Psychiatry* **198**:289–294. doi:10.1192/bjp.bp.109.076877

678 Bourgeron T. 2015. From the genetic architecture to synaptic plasticity in autism spectrum
679 disorder. *Nat Rev Neurosci* **16**:551–563. doi:10.1038/nrn3992

680 Chakrabarti S, Fombonne E. 2001. Pervasive Developmental Disorders in Preschool Children.
681 *JAMA* **285**:3093–3099. doi:10.1001/JAMA.285.24.3093

682 Cheng XT, Zhou B, Lin MY, Cai Q, Sheng ZH. 2015. Axonal autophagosomes recruit dynein
683 for retrograde transport through fusion with late endosomes. *J Cell Biol* **209**:377–386.
684 doi:10.1083/JCB.201412046/VIDEO-1

685 Courchesne E, Mouton PR, Calhoun ME, Semendeferi K, Ahrens-Barbeau C, Hallet MJ,
686 Barnes CC, Pierce K, PR M, PC B, MJ W, PR M, DC S, PO K, E C, E C, RA C, BF S, E
687 R, RA C, E C, HC H, G D, K C, CM S, HC H, E C, SJ W, E R, M S, DP K, H B, K S, G R,
688 GB S, PR M, VEB J, HBM U, RD B, CC L, JM G, T R, A C, WY K, D P, I K, JA H. 2011.
689 Neuron Number and Size in Prefrontal Cortex of Children With Autism. *JAMA* **306**:2001–
690 2010. doi:10.1001/jama.2011.1638

691 Delorme R, Ey E, Toro R, Leboyer M, Gillberg C, Bourgeron T. 2013. Progress toward
692 treatments for synaptic defects in autism. *Nat Med* **19**:685–694. doi:10.1038/nm.3193

693 Dere E, Dahm L, Lu D, Hammerschmidt K, Ju A, Tantra M, Kästner A, Chowdhury K,
694 Ehrenreich H, Kästner A, Chowdhury K, Ehrenreich H. 2014. Heterozygous Ambra1
695 Deficiency in Mice: A Genetic Trait with Autism-Like Behavior Restricted to the Female
696 Gender. *Front Behav Neurosci* **8**:181. doi:10.3389/fnbeh.2014.00181

697 Ebert DH, Greenberg ME. 2013. Activity-dependent neuronal signalling and autism spectrum
698 disorder. *Nature* **493**:327–337. doi:10.1038/nature11860

699 Elsabbagh M, Divan G, Koh Y-J, Kim YS, Kauchali S, Marcín C, Montiel-Navá C, Patel V,
700 Paula CS, Wang C, Yasamy MT, Fombonne E. 2012. Global Prevalence of Autism and
701 Other Pervasive Developmental Disorders. *Autism Res* **5**:160–179. doi:10.1002/aur.239

702 Epilepsy and autism spectrum disorders may have a shared aetiology. 2016. . *Nat Rev Neurol*
703 **12**:430–430. doi:10.1038/nrneurol.2016.100

704 Gkogkas CG, Khoutorsky A, Ran I, Rampakakis E, Nevarko T, Weatherill DB, Vasuta C, Yee
705 S, Truitt M, Dallaire P, Major F, Lasko P, Ruggero D, Nader K, Lacaille J-CC, Sonenberg
706 N. 2012. Autism-related deficits via dysregulated eIF4E-dependent translational control.
707 *Nature* **493**:371–377. doi:10.1038/nature11628

708 Hammer Matthieu, Krueger-Burg D, Tuffy Liam Patrick, Cooper BH, Taschenberger Holger,
709 Goswami Sarit Pati, Ehrenreich Hannelore, Jonas Peter, Varoqueaux Frederique, Rhee
710 J-S, Brose Nils, Bartos M, Vida I, Jonas P., Bemben MA, Nguyen Q-A, Wang T, Li Y,
711 Nicoll RA, Roche KW, Bolliger MF, Pei J, Maxeiner S, Boucard AA, Grishin NV, Südhof
712 TC, Braat S, Kooy RF, Bragin A, Jandó G, Nádasdy Z, Hetke J, Wise K, Buzsáki G, Cardin
713 JA, Carlén M, Meletis K, Knoblich U, Zhang F, Deisseroth K, Tsai L-H, Moore CI, Cellot
714 G, Cherubini E, Chanda S, Aoto J, Lee SJ, Wernig M, Südhof TC, Chao H-T, Chen H,
715 Samaco RC, Xue M, Chahrour M, Yoo J, Neul JL, Gong S, Lu H-C, Heintz N, al. et, Chen
716 JA, Peñagarikano O, Belgard TG, Swarup V, Geschwind DH, Chih B, Engelman H,
717 Scheiffele P, Delattre V, Mendola D La, Meystre J, Markram H, Markram K, El-Kordi A,
718 Winkler D, Hammerschmidt K, Kästner A, Krueger D, Ronnenberg A, Ritter C, Jatho J,
719 Radyushkin K, Bourgeron T, al. et, Fisahn A, Contractor A, Traub RD, Buhl EH,
720 Heinemann SF, McBain CJ, Fuchs EC, Zivkovic AR, Cunningham MO, Middleton S,
721 Lebeau FEN, Bannerman DM, Rozov A, Whittington MA, Traub RD, Rawlins JN, Monyer
722 H, Gogolla N, Leblanc JJ, Quast KB, Südhof TC, Fagiolini M, Hensch TK, Goswami S.P.,
723 Bucurenciu I, Jonas P., Hoon M, Soykan T, Falkenburger B, Hammer M., Patrizi A,
724 Schmidt KF, Sassoè-Pognetto M, Löwel S, Moser T, Taschenberger H., al. et, Jamain S,
725 Quach H, Betancur C, Råstam M, Colineaux C, Gillberg IC, Soderstrom H, Giros B,
726 Leboyer M, Gillberg C, Bourgeron T, Study PARIS, Jamain S, Radyushkin K,
727 Hammerschmidt K, Granon S, Boretius S, Varoqueaux F., Ramanantsoa N, Gallego J,
728 Ronnenberg A, Winter D, al. et, Jedlicka P, Hoon M, Papadopoulos T, Vlachos A, Winkels
729 R, Poulopoulos A, Betz H, Deller T, Brose N., Varoqueaux F., Schwarzacher SW, Ju A,
730 Hammerschmidt K, Tantra M, Krueger D, Brose N., Ehrenreich H., Katona L, Lapray D,
731 Viney TJ, Oulhaj A, Borhegyi Z, Micklem BR, Klausberger T, Somogyi P, Kerti-Szigeti K,
732 Nusser Z, Eyre MD, Kleijer KT, Schmeisser MJ, Krueger DD, Boeckers TM, Scheiffele P,
733 Bourgeron T, Brose N., Burbach JP, Krueger DD, Tuffy L.P., Papadopoulos T, Brose N.,
734 Lapray D, Lasztoczi B, Lagler M, Viney TJ, Katona L, Valenti O, Hartwich K, Borhegyi Z,

735 Somogyi P, Klausberger T, Laumonnier F, Bonnet-Brilhault F, Gomot M, Blanc R, David
736 A, Moizard M-P, Raynaud M, Ronce N, Lemonnier E, Calvas P, al. et, Mann EO, Paulsen
737 O, Maxwell CR, Villalobos ME, Schultz RT, Herpertz-Dahlmann B, Konrad K, Kohls G,
738 Möhler H, Pfeffer CK, Xue M, He M, Huang ZJ, Scanziani M, Poulopoulos A, Aramuni G,
739 Meyer G, Soykan T, Hoon M, Papadopoulos T, Zhang M, Paarmann I, Fuchs C, Harvey
740 K, al. et, Poulopoulos A, Soykan T, Tuffy L.P., Hammer M., Varoqueaux F., Brose N.,
741 Rothwell PE, Fuccillo MV, Maxeiner S, Hayton SJ, Gokce O, Lim BK, Fowler SC, Malenka
742 RC, Südhof TC, Rubenstein JLR, Merzenich MM, Sohal VS, Zhang F, Yizhar O,
743 Deisseroth K, Soykan T, Schneeberger D, Tria G, Buechner C, Bader N, Svergun D,
744 Tessmer I, Poulopoulos A, Papadopoulos T, Varoqueaux F., al. et, Südhof TC, Takács
745 VT, Szőnyi A, Freund TF, Nyiri G, Gulyás AI, Tyzio R, Nardou R, Ferrari DC, Tsintsadze
746 T, Shahrokhi A, Eftekhari S, Khalilov I, Tsintsadze V, Brouchoud C, Chazal G, al. et,
747 Uhlhaas PJ, Singer W, Varoqueaux F., Aramuni G, Rawson RL, Mohrmann R, Missler M,
748 Gottmann K, Zhang W, Südhof TC, Brose N., Voineagu I, Wang X, Johnston P, Lowe JK,
749 Tian Y, Horvath S, Mill J, Cantor RM, Blencowe BJ, Geschwind DH, Wolff SB,
750 Gründemann J, Tovote P, Krabbe S, Jacobson GA, Müller C, Herry C, Ehrlich I, Friedrich
751 RW, Letzkus JJ, Lüthi A, Yizhar O, Fenno LE, Prigge M, Schneider F, Davidson TJ,
752 O'Shea DJ, Sohal VS, Goshen I, Finkelstein J, Paz JT, al. et, Zhang C, Milunsky JM,
753 Newton S, Ko J, Zhao G, Maher TA, Tager-Flusberg H, Bolliger MF, Carter AS, Boucard
754 AA, al. et, Zoghbi HY. 2015. Perturbed Hippocampal Synaptic Inhibition and γ -
755 Oscillations in a Neuroligin-4 Knockout Mouse Model of Autism. *Cell Rep* **13**:516–23.
756 doi:10.1016/j.celrep.2015.09.011

757 Heiniger H. J. H-J, Dorey. 1989. Handbook on Genetically Standardized JAX Mice, 4th editio.
758 ed. The Jackson Laboratory, Bar Harbor.

759 Huang Y, Jiang H, Zheng Q, Fok AHK, Li X, Lau CG, Lai CSW. 2021. Environmental
760 enrichment or selective activation of parvalbumin-expressing interneurons ameliorates
761 synaptic and behavioral deficits in animal models with schizophrenia-like behaviors during
762 adolescence. *Mol Psychiatry* **26**:2533–2552. doi:10.1038/s41380-020-01005-w

763 Jockusch WJ, Speidel D, Sigler A, Sørensen JB, Varoqueaux F, Rhee J-S, Brose N. 2007.
764 CAPS-1 and CAPS-2 are essential synaptic vesicle priming proteins. *Cell* **131**:796–808.
765 doi:10.1016/j.cell.2007.11.002

766 Ju A, Fernandez-Arroyo B, Wu Y, Jacky D, Beyeler A. 2020. Expression of serotonin 1A and
767 2A receptors in molecular- And projection-defined neurons of the mouse insular cortex.
768 *Mol Brain* **13**:1–13.

769 Kawabe H, Neeb A, Dimova K, Young SM, Takeda M, Katsurabayashi S, Mitkovski M,
770 Malakhova OA, Zhang D-E, Umikawa M, Kariya K, Goebels S, Nave K-A, Rosenmund

771 C, Jahn O, Rhee J, Brose N. 2010. Regulation of Rap2A by the ubiquitin ligase Nedd4-1
772 controls neurite development. *Neuron* **65**:358–72. doi:10.1016/j.neuron.2010.01.007

773 Kuijpers M, Kochlamazashvili G, Stumpf A, Puchkov D, Swaminathan A, Lucht MT, Krause E,
774 Maritzen T, Schmitz D, Haucke V. 2021. Neuronal Autophagy Regulates Presynaptic
775 Neurotransmission by Controlling the Axonal Endoplasmic Reticulum. *Neuron* **109**:299–
776 313.e9. doi:10.1016/J.NEURON.2020.10.005

777 Lee BH, Smith T, Paciorkowski AR. 2015. Autism spectrum disorder and epilepsy: Disorders
778 with a shared biology. *Epilepsy Behav* **47**:191–201. doi:10.1016/J.YEBEH.2015.03.017

779 Lein ES, Hawrylycz MJ, Ao N, Ayres M, Bensinger A, Bernard A, Boe AF, Boguski MS,
780 Brockway KS, Byrnes EJ, Chen L, Chen L, Chen T-M, Chi Chin M, Chong J, Crook BE,
781 Czaplinska A, Dang CN, Datta S, Dee NR, Desaki AL, Desta T, Diep E, Dolbeare TA,
782 Donelan MJ, Dong H-W, Dougherty JG, Duncan BJ, Ebbert AJ, Eichele G, Estin LK, Faber
783 C, Facer BA, Fields R, Fischer SR, Fliss TP, Frenzley C, Gates SN, Glattfelder KJ,
784 Halverson KR, Hart MR, Hohmann JG, Howell MP, Jeung DP, Johnson RA, Karr PT,
785 Kawal R, Kidney JM, Knapik RH, Kuan CL, Lake JH, Laramee AR, Larsen KD, Lau C,
786 Lemon TA, Liang AJ, Liu Y, Luong LT, Michaels J, Morgan JJ, Morgan RJ, Mortrud MT,
787 Mosqueda NF, Ng LL, Ng R, Orta GJ, Overly CC, Pak TH, Parry SE, Pathak SD, Pearson
788 OC, Puchalski RB, Riley ZL, Rockett HR, Rowland SA, Royall JJ, Ruiz MJ, Sarno NR,
789 Schaffnit K, Shapovalova N V., Sivisay T, Slaughterbeck CR, Smith SC, Smith KA, Smith
790 BI, Sodt AJ, Stewart NN, Stumpf K-R, Sunkin SM, Sutram M, Tam A, Teemer CD, Thaller
791 C, Thompson CL, Varnam LR, Visel A, Whitlock RM, Wohnoutka PE, Wolkey CK, Wong
792 VY, Wood M, Yaylaoglu MB, Young RC, Youngstrom BL, Feng Yuan X, Zhang B,
793 Zwingman TA, Jones AR. 2007. Genome-wide atlas of gene expression in the adult
794 mouse brain. *Nature* **445**:168–176. doi:10.1038/nature05453

795 Li K, Nakajima M, Ibañez-Tallon I, Heintz N. 2016. A Cortical Circuit for Sexually Dimorphic
796 Oxytocin-Dependent Anxiety Behaviors. *Cell* **167**:60-72.e11.
797 doi:10.1016/j.cell.2016.08.067

798 Malishkevich A, Amram N, Hacohen-Kleiman G, Magen I, Giladi E, Gozes I. 2015. Activity-
799 dependent neuroprotective protein (ADNP) exhibits striking sexual dichotomy impacting
800 on autistic and Alzheimer's pathologies. *Transl Psychiatry* **5**:e501.
801 doi:10.1038/tp.2014.138

802 Maria Fimia G, Stoykova A, Romagnoli A, Giunta L, Di Bartolomeo S, Nardacci R, Corazzari
803 M, Fuoco C, Ucar A, Schwartz P, Gruss P, Piacentini M, Chowdhury K, Cecconi F. 2007.
804 Ambra1 regulates autophagy and development of the nervous system. *Nature* **447**:1121–
805 1125. doi:10.1038/nature05925

806 Martinerie J, Adam C, Quyen ML Van, Baulac M, Clemenceau S, Renault B, Varela FJ. 1998.
807 Epileptic seizures can be anticipated by non-linear analysis. *Nat Med* **4**:1173–1176.
808 doi:10.1038/2667

809 Mathalon DH, Sohal VS, G B, BJ R, RT C, J N, CA B, P T, Y H. 2015. Neural Oscillations and
810 Synchrony in Brain Dysfunction and Neuropsychiatric Disorders. *JAMA Psychiatry*
811 **72**:840–844. doi:10.1001/jamapsychiatry.2015.0483

812 Mitjans M, Begemann M, Ju A, Dere E, Wüstefeld L, Hofer S, Hassouna I, Balkenhol J, Oliveira
813 B, van der Auwera S, Tammer R, Hammerschmidt K, Völzke H, Homuth G, Cecconi F,
814 Chowdhury K, Grabe H, Frahm J, Boretius S, Dandekar T, Ehrenreich H. 2017. Sexual
815 dimorphism of AMBRA1-related autistic features in human and mouse. *Transl Psychiatry*
816 **7**:e1247–e1247. doi:10.1038/tp.2017.213

817 Nair R, Lauks J, Jung SY, Cooke NE, de Wit H, Brose N, Kilimann MW, Verhage M, Rhee JS.
818 2013. Neurobeachin regulates neurotransmitter receptor trafficking to synapses. *J Cell*
819 *Biol* **200**:61–80. doi:10.1083/JCB.201207113

820 Nelson SB, Valakh V. 2015. Excitatory/Inhibitory Balance and Circuit Homeostasis in Autism
821 Spectrum Disorders. *Neuron* **87**:684–698. doi:10.1016/j.neuron.2015.07.033

822 Ripamonti S, Ambrozkiewicz MC, Guzzi F, Gravati M, Biella G, Bormuth I, Hammer M, Tuffy
823 LP, Sigler A, Kawabe H, Nishimori K, Toselli M, Brose N, Parenti M, Rhee J. 2017.
824 Transient oxytocin signaling primes the development and function of excitatory
825 hippocampal neurons. *eLife* **6**. doi:10.7554/eLife.22466

826 Rodriguez A, Ehlenberger DB, Dickstein DL, Hof PR, Wearne SL. 2008. Automated Three-
827 Dimensional Detection and Shape Classification of Dendritic Spines from Fluorescence
828 Microscopy Images. *PLoS One* **3**:e1997. doi:10.1371/journal.pone.0001997

829 Rossi PG, Parmeggiani A, Bach V, Santucci M, Visconti P. 1995. EEG features and epilepsy
830 in patients with autism. *Brain Dev* **17**:169–174. doi:10.1016/0387-7604(95)00019-8

831 Sholl DA. 1953. Dendritic organization in the neurons of the visual and motor cortices of the
832 cat. *J Anat* **87**:387-406.1.

833 Sigler A, Oh WC, Imig C, Altas B, Kawabe H, Cooper BH, Kwon H-BB, Rhee J-SS, Brose N.
834 2017. Formation and Maintenance of Functional Spines in the Absence of Presynaptic
835 Glutamate Release. *Neuron* **94**:304-311.e4. doi:10.1016/j.neuron.2017.03.029

836 Soukup SF, Kuenen S, Vanhauwaert R, Manetsberger J, Hernández-Díaz S, Swerts J,
837 Schoovaerts N, Vilain S, Gounko N V., Vints K, Geens A, De Strooper B, Verstreken P.
838 2016. A LRRK2-Dependent EndophilinA Phosphoswitch Is Critical for Macroautophagy
839 at Presynaptic Terminals. *Neuron* **92**:829–844. doi:10.1016/J.NEURON.2016.09.037

840 Soykan T, Haucke V, Kuijpers M. 2021. Mechanism of synaptic protein turnover and its
841 regulation by neuronal activity. *Curr Opin Neurobiol* **69**:76–83.
842 doi:10.1016/J.CONB.2021.02.006

843 Spence SJ, Schneider MT. 2009. The Role of Epilepsy and Epileptiform EEGs in Autism
844 Spectrum Disorders. *Pediatr Res* **65**:599–606. doi:10.1203/PDR.0b013e31819e7168

845 Sun Y, Ren G, Ren J, Wang Q. 2021. High-frequency oscillations detected by
846 electroencephalography as biomarkers to evaluate treatment outcome, mirror
847 pathological severity and predict susceptibility to epilepsy. *Acta Epileptol* **3**:29.
848 doi:10.1186/s42494-021-00063-z

849 Tang G, Gudsnu K, Kuo S-HH, Cotrina MLL, Rosoklja G, Sosunov A, Sonders MSS, Kanter
850 E, Castagna C, Yamamoto A, Yue Z, Arancio O, Peterson BSS, Champagne F, Dwork
851 AJJ, Goldman J, Sulzer D. 2014. Loss of mTOR-Dependent Macroautophagy Causes
852 Autistic-like Synaptic Pruning Deficits. *Neuron* **83**:1131–1143.
853 doi:10.1016/j.neuron.2014.07.040

854 Vos T, Allen C, Arora M, Barber RM, Bhutta ZA, Brown A, Carter A, Casey DC, Charlson FJ,
855 Chen AZ, Coggeshall M, Cornaby L, Dandona L, Dicker DJ, Dilegge T, Erskine HE, Ferrari
856 AJ, Fitzmaurice C, Fleming T, Forouzanfar MH, Fullman N, Gething PW, Goldberg EM,
857 Graetz N, Haagsma JA, Hay SI, Johnson CO, Kassebaum NJ, Kawashima T, Kemmer L,
858 Khalil IA, Kinfu Y, Kyu HH, Leung J, Liang X, Lim SS, Lopez AD, Lozano R, Marczak L,
859 Mensah GA, Mokdad AH, Naghavi M, Nguyen G, Nsoesie E, Olsen H, Pigott DM, Pinho
860 C, Rankin Z, Reinig N, Salomon JA, Sandar L, Smith A, Stanaway J, Steiner C, Teeple
861 S, Thomas BA, Troeger C, Wagner JA, Wang H, Wanga V, Whiteford HA, Zoeckler L,
862 Abajobir AA, Abate KH, Abbafati C, Abbas KM, Abd-Allah F, Abraham B, Abubakar I,
863 Abu-Raddad LJ, Abu-Rmeileh NME, Ackerman IN, Adebiyi AO, Ademi Z, Adou AK, Afanvi
864 KA, Agardh EE, Agarwal A, Kiadaliri AA, Ahmadieh H, Ajala ON, Akinyemi RO, Akseer N,
865 Al-Aly Z, Alam K, Alam NKM, Aldhahri SF, Alegretti MA, Alemu ZA, Alexander LT, Alhabib
866 S, Ali R, Alkerwi A, Alla F, Allebeck P, Al-Raddadi R, Alsharif U, Altirkawi KA, Alvis-
867 Guzman N, Amare AT, Amberbir A, Amini H, Ammar W, Amrock SM, Andersen HH,
868 Anderson GM, Anderson BO, Antonio CAT, Aregay AF, Ärnlöv J, Artaman A, Asayesh H,
869 Assadi R, Atique S, Avokpaho EFGA, Awasthi A, Quintanilla BPA, Azzopardi P, Bacha U,
870 Badawi A, Balakrishnan K, Banerjee A, Barac A, Barker-Collo SL, Bärnighausen T,
871 Barregard L, Barrero LH, Basu A, Bazargan-Hejazi S, Beghi E, Bell B, Bell ML, Bennett
872 DA, Bensenor IM, Benzian H, Berhane A, Bernabé E, Betsu BD, Beyene AS, Bhala N,
873 Bhatt S, Biadgilign S, Bienhoff K, Bikbov B, Biryukov S, Bisanzio D, Bjertness E, Blore J,
874 Borschmann R, Boufous S, Brainin M, Brazinova A, Breitborde NJK, Brown J, Buchbinder
875 R, Buckle GC, Butt ZA, Calabria B, Campos-Nonato IR, Campuzano JC, Carabin H,

876 Cárdenas R, Carpenter DO, Carrero JJ, Castañeda-Orjuela CA, Rivas JC, Catalá-López
877 F, Chang J-C, Chiang PP-C, Chibueze CE, Chisumpa VH, Choi J-YJ, Chowdhury R,
878 Christensen H, Christopher DJ, Ciobanu LG, Cirillo M, Coates MM, Colquhoun SM,
879 Cooper C, Cortinovis M, Crump JA, Damtew SA, Dandona R, Daoud F, Dargan PI, das
880 Neves J, Davey G, Davis AC, Leo D De, Degenhardt L, Gobbo LC Del, Dellavalle RP,
881 Deribe K, Deribew A, Derrett S, Jarlais DC Des, Dharmaratne SD, Dhillon PK, Diaz-Torné
882 C, Ding EL, Driscoll TR, Duan L, Dubey M, Duncan BB, Ebrahimi H, Ellenbogen RG,
883 Elyazar I, Endres M, Endries AY, Ermakov SP, Eshrat B, Estep K, Farid TA, Farinha CS
884 e S, Faro A, Farvid MS, Farzadfar F, Feigin VL, Felson DT, Fereshtehnejad S-M,
885 Fernandes JG, Fernandes JC, Fischer F, Fitchett JRA, Foreman K, Fowkes FGR, Fox J,
886 Franklin RC, Friedman J, Frostad J, Fürst T, Futran ND, Gabbe B, Ganguly P, Gankpé
887 FG, Gebre T, Gebrehiwot TT, Gebremedhin AT, Geleijnse JM, Gessner BD, Gibney KB,
888 Ginawi IAM, Giref AZ, Giroud M, Gishu MD, Giussani G, Glaser E, Godwin WW, Gomez-
889 Dantes H, Gona P, Goodridge A, Gopalani SV, Gotay CC, Goto A, Gouda HN, Grainger
890 R, Greaves F, Guillemin F, Guo Y, Gupta Rahul, Gupta Rajeev, Gupta V, Gutiérrez RA,
891 Haile D, Hailu AD, Hailu GB, Halasa YA, Hamadeh RR, Hamidi S, Hammami M, Hancock
892 J, Handal AJ, Hankey GJ, Hao Y, Harb HL, Harikrishnan S, Haro JM, Havmoeller R, Hay
893 RJ, Heredia-Pi IB, Heydarpour P, Hoek HW, Horino M, Horita N, Hosgood HD, Hoy DG,
894 Htet AS, Huang H, Huang JJ, Huynh C, Iannarone M, Iburg KM, Innos K, Inoue M, Iyer
895 VJ, Jacobsen KH, Jahanmehr N, Jakovljevic MB, Javanbakht M, Jayaraman SP,
896 Jayatilleke AU, Jee SH, Jeemon P, Jensen PN, Jiang Y, Jibat T, Jimenez-Corona A, Jin
897 Y, Jonas JB, Kabir Z, Kalkonde Y, Kamal R, Kan H, Karch A, Karema CK, Karimkhani C,
898 Kasaeian A, Kaul A, Kawakami N, Keiyoro PN, Kemp AH, Keren A, Kesavachandran CN,
899 Khader YS, Khan AR, Khan EA, Khang Y-H, Khera S, Khoja TAM, Khubchandani J,
900 Kieling C, Kim P, Kim C, Kim D, Kim YJ, Kissoon N, Knibbs LD, Knudsen AK, Kokubo Y,
901 Kolte D, Kopec JA, Kosen S, Kotsakis GA, Koul PA, Koyanagi A, Kravchenko M, Defo
902 BK, Bicer BK, Kudom AA, Kuipers EJ, Kumar GA, Kutz M, Kwan GF, Lal A, Laloo R,
903 Lallukka T, Lam H, Lam JO, Langan SM, Larsson A, Lavados PM, Leasher JL, Leigh J,
904 Leung R, Levi M, Li Yichong, Li Yongmei, Liang J, Liu S, Liu Y, Lloyd BK, Lo WD,
905 Logroscino G, Looker KJ, Lotufo PA, Lunevicius R, Lyons RA, Mackay MT, Magdy M,
906 Razek A EI, Mahdavi M, Majdan M, Majeed A, Malekzadeh R, Marcenes W, Margolis DJ,
907 Martinez-Raga J, Masiye F, Massano J, McGarvey ST, McGrath JJ, McKee M, McMahon
908 BJ, Meaney PA, Mehari A, Mejia-Rodriguez F, Mekonnen AB, Melaku YA, Memiah P,
909 Memish ZA, Mendoza W, Meretoja A, Meretoja TJ, Mhimbira FA, Millear A, Miller TR,
910 Mills EJ, Mirarefin M, Mitchell PB, Mock CN, Mohammadi A, Mohammed S, Monasta L,
911 Hernandez JCM, Montico M, Mooney MD, Moradi-Lakeh M, Morawska L, Mueller UO,

912 Mullany E, Mumford JE, Murdoch ME, Nachege JB, Nagel G, Naheed A, Naldi L, Nangia
913 V, Newton JN, Ng M, Ngalesoni FN, Nguyen Q Le, Nisar MI, Pete PMN, Nolla JM,
914 Norheim OF, Norman RE, Norrving B, Nunes BP, Ogbo FA, Oh I-H, Ohkubo T, Olivares
915 PR, Olusanya BO, Olusanya JO, Ortiz A, Osman M, Ota E, PA M, Park E-K, Parsaeian
916 M, de Azeredo Passos VM, Caicedo AJP, Patten SB, Patton GC, Pereira DM, Perez-
917 Padilla R, Perico N, Pesudovs K, Petzold M, Phillips MR, Piel FB, Pillay JD, Pishgar F,
918 Plass D, Platts-Mills JA, Polinder S, Pond CD, Popova S, Poulton RG, Pourmalek F,
919 Prabhakaran D, Prasad NM, Qorbani M, Rabiee RHS, Radfar A, Rafay A, Rahimi K,
920 Rahimi-Movaghar V, Rahman M, Rahman MHU, Rahman SU, Rai RK, Rajsic S, Ram U,
921 Rao P, Refaat AH, Reitsma MB, Remuzzi G, Resnikoff S, Reynolds A, Ribeiro AL,
922 Blancas MJR, Roba HS, Rojas-Rueda D, Ronfani L, Roshandel G, Roth GA,
923 Rothenbacher D, Roy A, Sagar R, Sahathevan R, Sanabria JR, Sanchez-Niño MD,
924 Santos IS, Santos JV, Sarmiento-Suarez R, Sartorius B, Satpathy M, Savic M, Sawhney
925 M, Schaub MP, Schmidt MI, Schneider IJC, Schöttker B, Schwebel DC, Scott JG, Seedat
926 S, Sepanlou SG, Servan-Mori EE, Shackelford KA, Shaheen A, Shaikh MA, Sharma R,
927 Sharma U, Shen J, Shepard DS, Sheth KN, Shibuya K, Shin M-J, Shiri R, Shiue I, Shrime
928 MG, Sigfusdottir ID, Silva DAS, Silveira DGA, Singh A, Singh JA, Singh OP, Singh PK,
929 Sivonda A, Skirbekk V, Skogen JC, Sligar A, Sliwa K, Soljak M, Søreide K, Sorensen RJD,
930 Soriano JB, Sposato LA, Sreeramareddy CT, Stathopoulou V, Steel N, Stein DJ, Steiner
931 TJ, Steinke S, Stovner L, Stroumpoulis K, Sunguya BF, Sur P, Swaminathan S, Sykes
932 BL, Szoke CEI, Tabarés-Seisdedos R, Takala JS, Tandon N, Tanne D, Tavakkoli M,
933 Taye B, Taylor HR, Ao BJ Te, Tedla BA, Terkawi AS, Thomson AJ, Thorne-Lyman AL,
934 Thrift AG, Thurston GD, Tobe-Gai R, Tonelli M, Topor-Madry R, Topouzis F, Tran BX,
935 Truelsen T, Dimbuene ZT, Tsilimbaris M, Tura AK, Tuzcu EM, Tyrovolas S, Ukwaja KN,
936 Undurraga EA, Uneke CJ, Uthman OA, van Gool CH, Varakin YY, Vasankari T,
937 Venketasubramanian N, Verma RK, Violante FS, Vladimirov SK, Vlassov VV, Vollset SE,
938 Wagner GR, Waller SG, Wang L, Watkins DA, Weichenthal S, Weiderpass E, Weintraub
939 RG, Werdecker A, Westerman R, White RA, Williams HC, Wiysonge CS, Wolfe CDA,
940 Won S, Woodbrook R, Wubshet M, Xavier D, Xu G, Yadav AK, Yan LL, Yano Y, Yaseri
941 M, Ye P, Yebyo HG, Yip P, Yonemoto N, Yoon S-J, Younis MZ, Yu C, Zaidi Z, Zaki MES,
942 Zeeb H, Zhou M, Zodpey S, Zuhlke LJ, Murray CJL. 2016. Global, regional, and national
943 incidence, prevalence, and years lived with disability for 310 diseases and injuries, 1990–
944 2015: a systematic analysis for the Global Burden of Disease Study 2015. *Lancet*
945 **388**:1545–1602. doi:10.1016/S0140-6736(16)31678-6
946 Wang T, Martin S, Papadopoulos A, Harper CB, Mavlyutov TA, Niranjan D, Glass NR, Cooper-
947 White JJ, Sibarita JB, Choquet D, Davletov B, Meunier FA. 2015. Control of

948 Autophagosome Axonal Retrograde Flux by Presynaptic Activity Unveiled Using
949 Botulinum Neurotoxin Type A. *J Neurosci* **35**:6179–6194.
950 doi:10.1523/JNEUROSCI.3757-14.2015

951 Wojcik SMSM, Tantra M, Stepniak B, Man MK-N, Müller-Ribbe K, Begemann M, Ju A, Papiol
952 S, Ronnenberg A, Gurvich A, Shin Y, Augustin I, Brose N, Ehrenreich H, Man K-NM,
953 Müller-Ribbe K, Begemann M, Ju A, Papiol S, Ronnenberg A, Gurvich A, Shin Y, Augustin
954 I, Brose N, Ehrenreich H. 2013. Genetic markers of a Munc13 protein family member,
955 BAIAP3, are gender specifically associated with anxiety and benzodiazepine abuse in
956 mice and humans. *Mol Med* **19**:135–148. doi:10.2119/molmed.2013.00033

957 Xue M, Atallah B V., Scanziani M. 2014. Equalizing excitation–inhibition ratios across visual
958 cortical neurons. *Nature* **511**:596–600. doi:10.1038/nature13321

959 Zikopoulos B, Barbas H. 2013. Altered neural connectivity in excitatory and inhibitory cortical
960 circuits in autism. *Front Hum Neurosci* **7**:609. doi:10.3389/fnhum.2013.00609

961

962

963 **Supplemental Information**

964

965 **Developmental features in this mouse line**

966 A previous publication has reported alterations in synaptic plasticity, pyramidal neuron spine
967 density and number of parvalbumin-expressing neurons in the hippocampus of adult mice (8
968 weeks old) restricted to females, whereas we observed no difference in our 4 week-old mice
969 (Nobili et al., 2018). Therefore, we hypothesized that the developmental stage is a pivotal factor
970 to explain the neural substrate underlying and the prepubertal stage is very critical time window
971 in this mouse line. We previously reported very interesting developmental features in seizure
972 propensity, showing opposite transition from protective response to seizure induction in female
973 mutants of 3 weeks old to reduced survival in 13 months old (Mitjans et al., 2017). Here, we
974 added seizure susceptibility at 12 weeks old where this transition already happened, indicating
975 developmental progression of seizure propensity in this mouse line (Mitjans et al., 2017).

976

977

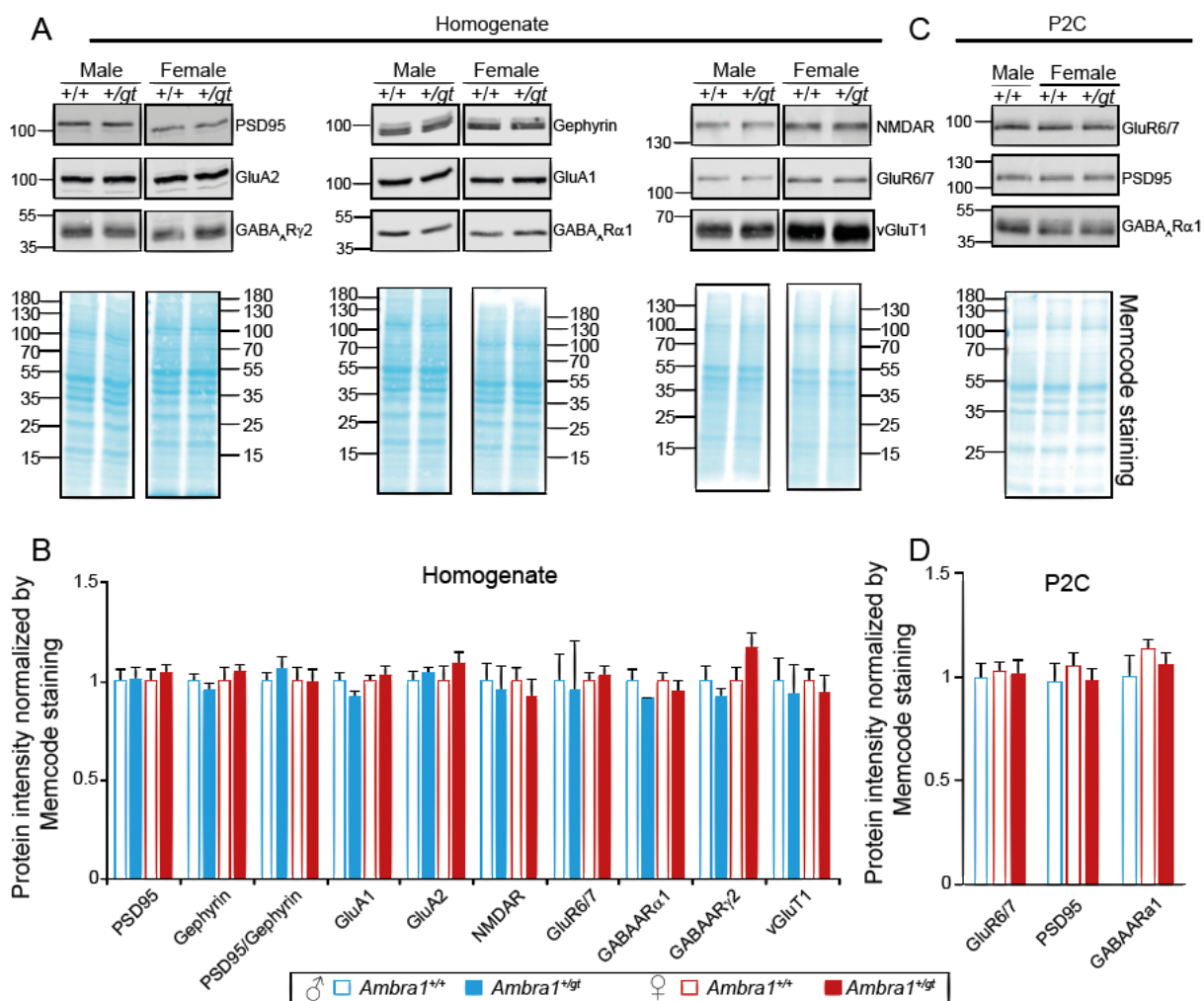
978 **Reference**

979 Mitjans M, Begemann M, Ju A, Dere E, Wüstefeld L, Hofer S, Hassouna I, Balkenhol J,
980 Oliveira B, van der Auwera S, Tammer R, Hammerschmidt K, Völzke H, Homuth G,
981 Cecconi F, Chowdhury K, Grabe H, Frahm J, Boretius S, Dandekar T, Ehrenreich H.
982 2017. Sexual dimorphism of AMBRA1-related autistic features in human and mouse.
983 *Transl Psychiatry* 7:e1247–e1247. doi:10.1038/tp.2017.213

984 Nobili A, Krashia P, Cordella A, La Barbera L, Dell'Acqua MC, Caruso A, Pignataro A, Marino
985 R, Sciarra F, Biamonte F, Scattoni ML, Ammassari-Teule M, Cecconi F, Berretta N,
986 Keller F, Mercuri NB, D'Amelio M. 2018. Ambra1 Shapes Hippocampal
987 Inhibition/Excitation Balance: Role in Neurodevelopmental Disorders. *Mol Neurobiol*
988 55:7921–7940. doi:10.1007/s12035-018-0911-5

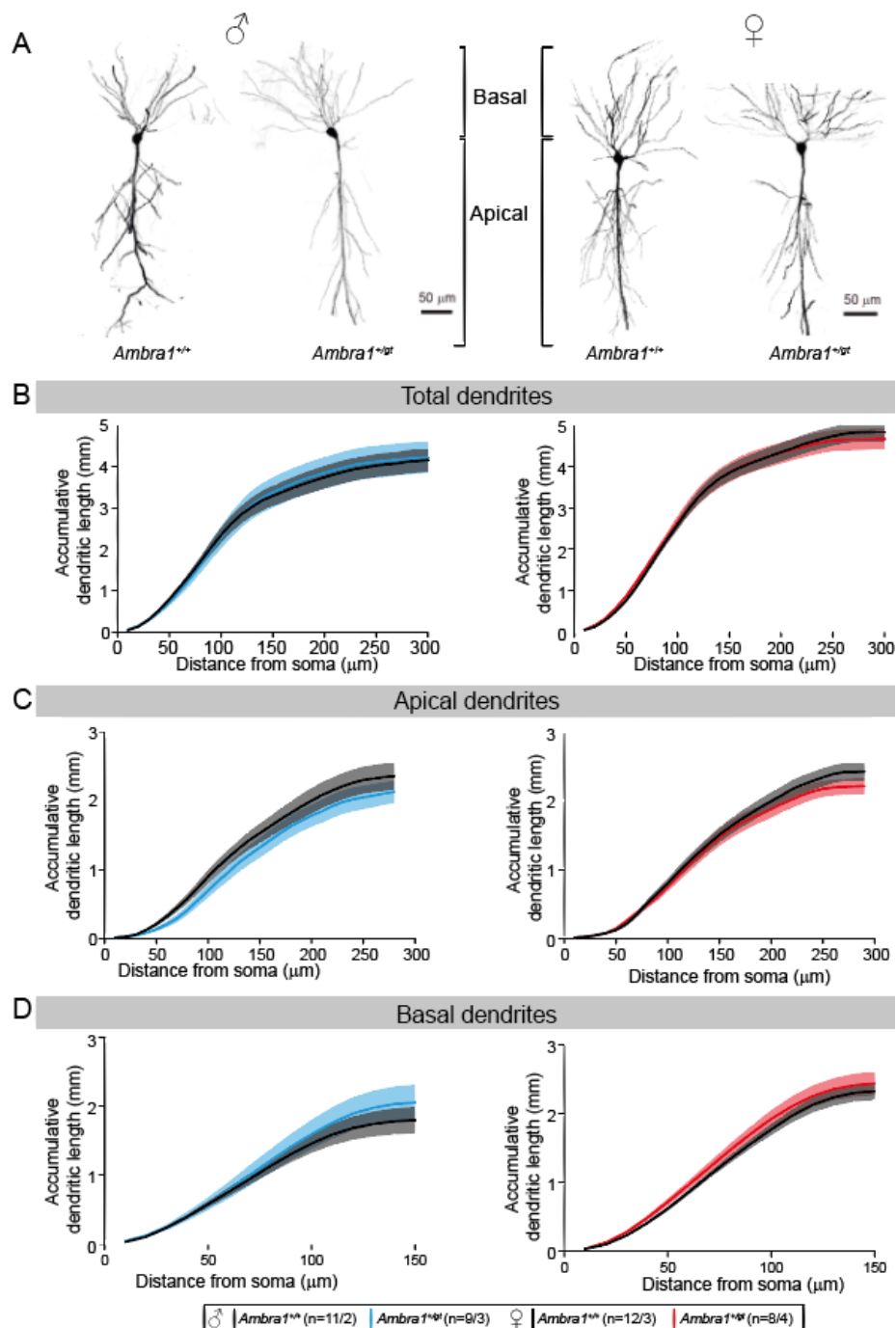
989

990



992 **Supplementary Figure S1: Quantification of synaptic proteins in homogenate and**
 993 **synaptosomes**

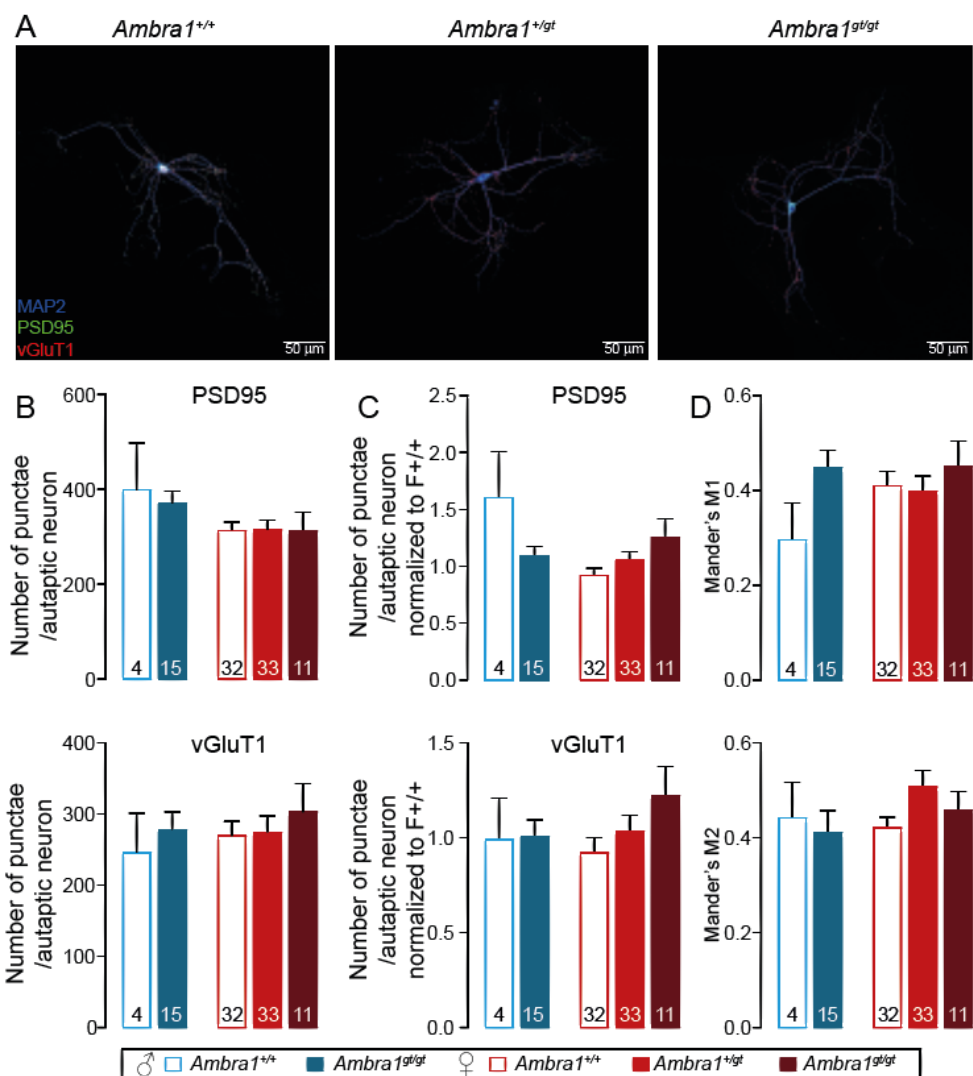
994 Sample pictures of synaptic proteins (**A, C**) and corresponding Memcode staining and their
 995 quantification (**B, D**) were obtained from hippocampal homogenates of *Ambra1*^{+/+} (+/+) and
 996 *Ambra1*^{+gt} (+/gt) in 4 week-old males and females (**A, B**) and cortical P2C of 6 week-old male
 997 +/+ and female +/+ and +/gt (**C, D**). The intensity of synaptic proteins was normalized by
 998 corresponding MemCode staining as the amount of total proteins and normalized by the
 999 average value of male wild-type group. 3-7 mice were used per each group. The bar graphs
 1000 represent mean \pm S.E.M and statistical analysis between two genotypes were carried out by
 1001 two-tailed unpaired t-test with significance level $p < 0.05$.



1002

1003 **Supplementary Figure S2: Sholl analysis from *in utero* electroporated neurons**

1004 Data from male and female mice are placed on the left and right side, respectively. **A**
1005 Representative picture of CA1 pyramidal neurons in hippocampus of *Ambra1^{+/+}* and *Ambra1^{+gt}*
1006 mice in males and females at P28. **B-D** Comparison of dendritic length in whole (B), apical (C)
1007 and basal (D) parts of pyramidal neurons in every 10 μm between genotypes in male and
1008 female, separately. Neuron number/animal number are written next to the legends. Mean \pm
1009 S.E.M. are presented in line and area and statistical difference was defined by p-value between
1010 genotypes from Repeated-Measures of ANOVA.



1011

1012 **Supplementary Figure S3: Quantification of synapse number in glutamatergic autaptic**
 1013 **hippocampal neurons**

1014 **A** Representative images of glutamatergic autaptic neurons from *Ambr1^{+/+}*, *Ambr1^{+gt}* and
 1015 *Ambr1^{gt/gt}* of E14.5 female hippocampi-like structures stained with antibodies against vGluT1,
 1016 PSD95 and MAP2 at DIV18-23. **B, C** The absolute (**B**) or normalized number (**C**) of pre-
 1017 (vGluT1-positive, above) or post-synaptic (PSD95-positive, below) puncta are shown. The
 1018 normalization was done by dividing the average value of female *Ambr1^{+/+}* cultured on the
 1019 same day. **D** M1 (above) and M2 (below) coefficient of Mander's overlapping analysis between
 1020 vGluT1 and PSD95 signals. The bar graphs represent mean \pm S.E.M and the numbers of
 1021 analyzed neurons are written inside the bottom of each bar. Statistical analysis between
 1022 genotypes were carried out by two-way ANOVA followed by post-hoc Bonferroni test with
 1023 significance level $p < 0.05$.